Published in final edited form as:
*Nat Microbiol*. 2021 August 01; 6(8): 1031–1042. doi:10.1038/s41564-021-00937-5.

# MX2-mediated innate immunity against HIV-1 is regulated by serine phosphorylation

**Gilberto Betancor**[1,*], **Jose M Jimenez-Guardeño**[1], **Steven Lynham**[2], **Robin Antrobus**[3], **Hataf Khan**[1], **Andrew Sobala**[1], **Matthew DJ Dicks**[1], **Michael H Malim**[1,*]

[1]Department of Infectious Diseases, School of Immunology & Microbial Sciences, King's College London, London SE1 9RT, UK

[2]Centre of Excellence for Mass Spectrometry, The James Black Centre, King's College London, London SE5 9NU, UK

[3]Cambridge Institute for Medical Research, Department of Medicine, University of Cambridge, Cambridge CB2 0XY, UK

## Abstract

The antiviral cytokine interferon (IFN) activates expression of IFN-stimulated genes (ISGs) to establish an antiviral state. Myxovirus resistance 2 (MX2/MxB) is an ISG that inhibits the nuclear import of HIV-1 and interacts with the viral capsid and cellular nuclear transport machinery. We identified the myosin light chain phosphatase (MLCP) subunits MYPT1 and PPP1CB as positively-acting regulators of MX2, interacting with its N-terminal domain (NTD). We demonstrated that serine phosphorylation of the NTD at positions 14, 17 and 18 suppresses MX2 antiviral function, prevents interactions with the HIV-1 capsid and nuclear transport factors, and is reversed by MLCP. Importantly, NTD serine phosphorylation also impedes MX2-mediated inhibition of nuclear import of cellular karyophilic cargo. We additionally found that IFN treatment reduces levels of phosphorylation at these serines and outline a homeostatic regulatory mechanism where repression of MX2 by phosphorylation, together with MLCP-mediated dephosphorylation, balances the deleterious effects of MX2 upon normal cell function with innate immunity against HIV-1.

## Introduction

Type 1 interferons (IFNs) are produced following recognition of pathogen-associated markers by cell-encoded pattern recognition receptors. In response to IFN, a set of genes

[*]Co-corresponding authors: Department of Infectious Diseases, School of Immunology & Microbial Sciences, King's College London, 2nd Floor Borough Wing, Guy's Hospital, London Bridge, London, SE1 9RT tel: +44 20 7848 9606, michael.malim@kcl.ac.uk, gilberto.betancor@kcl.ac.uk.

**Author contributions**

GB and MHM designed the study and wrote the manuscript with input from all co-authors; GB carried out the experiments and analyzed the data, with contributions from AES in figure 1, MDJD in figure 2, JMJ-G in figure 3, 5 and figure S2, SL in figure 1 and RA in figure 4; AES, MDJD and JMJ-G contributed to the execution of experiments and provided reagents; and, MHM supervised all aspects of the project.

**Conflict of interest**

The authors declare that they have no conflict of interest.


Europe PMC Funders Author Manuscripts

known as IFN stimulated genes (ISGs) are transcribed, which establishes an antiviral state within the infected host[1,2]. Myxovirus resistance 2 (MX2/MxB) is an ISG with potent inhibitory activity against HIV-1 as well as herpesviruses and hepatitis B virus (HBV)[3–10]. MX2 inhibits HIV-1 infection prior to the nuclear import of viral pre-integration complexes, but after reverse transcription[3,4,11]. Point mutations in the Capsid (CA) protein can render the virus insensitive to MX2, linking MX2 function to recognition of the capsid lattice [3–5,12,13].

MX2 belongs to the dynamin-like family of GTPases and is closely related to MX1 (MxA), another ISG that has broad inhibitory activity for a variety of RNA and DNA viruses, including influenza A virus (IAV) and HBV[14–16]. Unlike MX1, where a conserved loop in the stalk domain (loop 4) is critical for restriction of IAV[17–20], the amino-terminal domain (NTD) is the principal determinant of MX2's activity against HIV-1[21,23]. For instance, transfer of this domain to unrelated proteins confers HIV-1 inhibitory activity on them[21–25]. The NTD also determines the localization of MX2 to the nuclear envelope[25,26]. Three conserved arginine residues at positions 11 to 13 in the NTD have been shown to be required for antiviral activity[25,26], to be important for CA binding[27–29], and to be involved in interactions with nuclear transport factors including nuclear pore proteins such as NUP214 and the nuclear transport receptor transportin 1 (TNPO1)[25].

Here, we identify cellular proteins that interact with the NTD, and examine how they regulate MX2-mediated inhibition of HIV-1 nuclear import. In so doing, a cellular mechanism for regulating the deleterious effects of MX2 on nuclear trafficking in cells in the absence of virus infection is revealed.

## Results

### The N-terminal domain of MX2 interacts with MYPT1 and PPP1CB

To understand in greater detail the mechanistic basis for MX2 function, we used the retrieval of tagged proteins from transfected 293T cells to identify interacting cellular proteins. Specifically, we performed SILAC-based screens with a series of MX protein and control constructs that enabled four pairwise comparisons: MX2 versus MX1, MX2 versus mock transfection, MX2 versus a non-functional mutant where the arginines at positions 11 to 13 had been replaced with alanine (R11-13A)[23], and green fluorescent protein (GFP) versus a GFP ($NTD_{MX2}$) chimaera. Two interacting proteins were consistently enriched in samples obtained using proteins bearing the wild type MX2 NTD (i.e., MX2 and GFP ($NTD_{MX2}$)): myosin phosphatase target subunit 1 (MYPT1) and protein phosphatase 1 catalytic subunit beta (PPP1CB) (Fig. 1a). As expected, owing to its ability to oligomerize[24,30], MX2 itself was also enriched in all comparisons except MX2 vs MX2 R11-13A.

MYPT1 and PPP1CB, together with the small subunit M20, assemble to form a holoenzyme known as myosin light chain phosphatase (MLCP), a member of the serine/threonine protein phosphatase 1 (PP1) family[31]. For this holoenzyme, PPP1CB is the catalytic subunit (PP1c), while MYPT1 serves as a regulatory factor. PP1 complexes are able to interact with their substrates through a variety of motifs[32]. One of these, comprising the sequence F-X-X-R-X-R, has been found in the cytosolic RNA sensors MDA5 and RIG-I, and acts as a binding

site for other PP1 catalytic subunits (PPP1CA and PPP1CC)[33]. Notably, a variant of this motif ($^{8}$W-P-Y-R-R-R$^{13}$) is present in the MX2 NTD (Fig. 1b) and harbours the three arginines at positions 11, 12 and 13, explaining why MYPT1 and PPP1CB were enriched for binding to wild type MX2 relative to MX2 R11-13A (Fig. 1a). Additional confirmation of this interaction was obtained in co-immunoprecipitation experiments where MX2 and GFP ($NTD_{MX2}$), but not MX1, MX2 R11-13A or GFP ($NTD_{MX2}$) R11-13A were able to pull-down endogenous PPP1CB and MYPT1(Fig. 1c).

## MLCP regulates the antiviral activity of MX2

We next addressed the impact of MLCP on the antiviral activity of MX2. U87-MG CD4$^{+}$ CXCR4$^{+}$ cells, a well-stablished *in vitro* model for studying HIV-1 replication[3, 9, 21, 23–25, 28], expressing MX2 or the control protein luciferase (Luc) were transfected with pools of four siRNAs directed against PPP1CB or MYPT1, or a control (CTR) siRNA. In cells treated with CTR siRNA, infection with an HIV-1 based lentiviral vector (HIV-1/GFP) was ~10-fold lower in cells expressing MX2 (Fig. 2a), consistent with previous data[21,23–25]. In cells depleted of PPP1CB or MYPT1 the suppressive effect of MX2 was reduced to ~5-fold; the partial nature of these effects is likely attributable to incomplete silencing (Fig. 2b). Analysis of individual constituent siRNAs yielded variable results with one MYPT1 and two PPP1CB siRNAs recapitulating the phenotypes of the pools (Extended data Fig. 1a). Critically, increases in infection were not observed following MYPT1 or PPP1CB silencing in the presence of MX2 when cells were challenged with MX2-insensitive viruses based on murine leukemia virus (MLV) or bearing the MX2-resistant HIV-1 CA mutation P90A (Fig. 2a). Additionally, cells doubly depleted of PPP1CB and MYPT1 did not display a further loss of MX2 antiviral activity, relative to individual knock-downs, suggestive of their activities being mediated through a common pathway (Extended data Fig. 1b). Finally, ectopic expression of MYPT1, but not PPP1CB, in MX2 expressing U87-MG CD4$^{+}$ CXCR4$^{+}$ cells reduced the inhibitory effect of MX2 (Extended data Fig. 2a), an effect likely due to the ability of ectopically expressed MYPT1 to impair the interaction of MX2 with endogenous PPP1CB (Extended data Fig. 2b). Such dominant-negative behaviour further links MYPT1/MLCP function to the antiviral activity of MX2.

There are several pharmacologic inhibitors of protein phosphatases. Okadaic acid inhibits both PP1 and PP2 (the other main serine/threonine protein phosphatase) but is far more potent against the latter ($IC_{50}$ values ranging from 60 to 500 nM, versus 1 nM, respectively). Calyculin A has a similar activity profile for both ($IC_{50}$ of 0.5-1 nM) and therefore inhibits PP1 at lower concentrations than okadaic acid. Finally, rubratoxin A is a PP2 specific inhibitor[34–38]. Concentrations of calyculin A as low as 2.25 nM yielded significant reductions in MX2 activity (Fig. 2c), whereas much higher concentrations of okadaic acid (from 30 nM) were required to produce a similar effect and even the highest tested concentration of rubratoxin A (50 μM) had no effect. Finally, the specificity of these drug effects was confirmed in MLV challenges of U87-MG CD4$^{+}$ CXCR4$^{+}$ cells where any viral suppression was equivalent in Luc or MX2 expressing cells at all concentrations tested (Extended data Fig. 2c). Altogether, these data implicate MLCP, a PP1, as a novel regulator of MX2-mediated HIV-1 inhibition.

## MX2 requires functional MLCP to inhibit viral infection

We then asked whether endogenous MX2 (expressed following IFN exposure) is regulated by MLCP. We used bulk and clonal cell populations (two) derived from U87-MG $CD4^+$ $CXCR4^+$ cells where the endogenous *MX2* alleles had been inactivated using CRISPR-Cas9 genome editing, as well as a control line (CTR CRISPR)[25]. Cells were transfected with siRNAs specific for MX2 (positive control), MYPT1, or PPP1CB, or a CTR siRNA, before being incubated for 24 h in the presence or absence of IFN. As previously established, IFN-mediated viral suppression was severely impaired in all three MX2 knock-out cultures compared to CTR CRISPR cells (~3-fold reduction in infection compared to ~12-fold, respectively) (Fig. 3a). Critically, significant losses in the antiviral activity of IFN were apparent when MYPT1 or PPP1CB were depleted in CTR cells, but this ameliorating effect was dependent on MX2-mediated suppression and was not therefore seen in any of the *MX2*-knock-out lines (Fig. 3b shows corresponding analyses of protein levels). Complementing these data, calyculin A also partially reversed the effect of IFN, but again this was limited to CTR cells and not cells lacking MX2. (Fig. 3a). Of note, and consistent with earlier findings (Fig. 2a), the modest inhibition of MLV infection by IFN was unaffected by the absence of MX2 or by the depletion of MYPT1 or PPP1CB, again associating MX2 function with MLCP activity (Extended data Fig. 3).

We next addressed whether MYPT1 and PPP1CB contribute to the IFN-induced suppression of HIV-1 in primary human $CD4^+$ T cells, the principal target of viral infection *in vivo*. Short hairpin RNAs (shRNAs) specific for MX2, MYPT1 or PPP1CB as well as a negative control (scrambled sequence) were delivered by lentiviral vector transduction. In all four donors, depletion of any of these genes resulted in reduced inhibition of HIV-1 by IFN (Fig. 3c; Fig. 3d shows the mRNA levels). Similarly, inhibition of PP1 using calyculin A reduced the antiviral effect of IFN in all seven donors analyzed (Fig. 3e). These findings confirm the role of MLCP in the IFN-mediated inhibition of HIV-1 and demonstrate that their activity is channeled through MX2.

## MX2 antiviral activity is regulated by serine phosphorylation

Based on the aforementioned data, we predicted that MLCP dephosphorylates functionally important residues in the MX2 NTD. We therefore used LC-MS/MS to identify post-translational modifications in MX2 expressed in 293T cells. By focusing on the NTD, we identified modified peptides that revealed that MX2 is phosphorylated at the serines at positions 14, 17, 18, 28 and 78, and the threonines at 38 and 67 (Fig. 4a; (Extended data Fig. 4a). While 99% of MX2's sequence was covered by multiple peptides, peptides corresponding to the amino-terminal 20 amino acids were underrepresented. Critically, of the 42 peptides identified within this N-terminal region, 19 were phosphorylated at positions 14, 17 or 18. Owing to the close proximity of these modified residues, often lying within a single LysC digested peptide, estimates of relative peptide abundances were therefore calculated using chromatographic peak areas (Extended data Fig. 4b): it is apparent that all three serines are frequently phosphorylated when comparing areas from unmodified peptide with phosphorylated ones, especially S14.

We next explored the biological impact of these findings by replacing the seven serine/threonine residues (individually or in combination for S14, S17 and S18) with alanine to block phosphorylation, or with the phosphomimetic aspartic acid (Fig. 4b). All mutations of S28, T38, T67 or S78 maintained strong HIV-1 inhibitory activity indicating that phosphorylation at these positions does not diminish function (Fig. 4b). In contrast, the triple S14, 17-18D mutation (which we suggest equates to a MLCP-null scenario) rendered MX2 inactive whereas the triple-alanine substitution was as active as the wild type protein. Further corroboration of this phenotype was obtained with the chimeric proteins MX1 ($NTD_{MX2}$) or Fv1b ($NTD_{MX2}$), which were also inactive when bearing the S14, 17-18D substitutions (Extended data Fig. 5a). Individual substitutions of S14, S17 or S18 with aspartic acid yielded proteins with intermediate antiviral phenotypes, while double substitutions of residues 14 and 17 or 14 and 18, but not as evidently 17 and 18, produced proteins with virtually no antiviral activity (Extended data Fig. 5b).

Owing to the functional importance of phosphorylation at these three serines, we generated a polyclonal antiserum using a peptide antigen containing S14, S17 and S18 in their phosphorylated form. This antiserum (anti-P-NTD) detects wild type MX2 and all proteins with at least one aspartic acid substitution, but not the version with the triple S14, 17-18A substitution (Fig. 4c). Importantly, we were able to use this antiserum to confirm that depletion of PPP1CB with siRNA (Fig. 4d), or inactivation by treatment with calyculin A (Fig. 4e), directly increased the level of phosphorylation of the S14-S17-S18 motif (~3-fold and ~5-fold, respectively). As controls, detection of the MX2 S14, 17-18D was noted as being unaffected by altering MLCP activity.

To link further MLCP function with MX2 antiviral activity, we depleted PPP1CB from U87-MG $CD4^+$ $CXCR4^+$ cells expressing wild type MX2 or the S14, 17-18A derivative and determined the ability of these proteins to inhibit HIV-1 infection relative to cells receiving control siRNA. Consistent with our previous data, PPP1CB depletion only reduced the antiviral activity of MX2, while the S14, 17-18A mutant was unaffected (Fig. 4f). These results therefore confirm the role of MLCP as a key regulator of the phosphorylation status and antiviral activity of MX2.

## Serine phosphorylation prevents MX2 NTD-HIV-1 capsid interaction

Having revealed the importance of phosphorylation at positions 14, 17 and 18 for neutralizing MX2 antiviral activity, it was important to assess effects on ligand interactions. We and others have previously shown that MX2 specifically interacts with CA and capsid-nucleocapsid (CANC) assemblies *in* vitro[22,28,29,39]; we therefore used CANC complexes and whole cell lysates from transfected 293T cells expressing MX1 (negative control), wild type MX2 or the S14, 17-18D mutant to examine CA binding. As seen in the pellet samples, phosphorylation at these positions severely inhibited binding to CA (Fig. 5a), however, presumably due to the second CA-interacting domain in the G domain of MX2[28], binding was not fully abolished. Introduction of these substitutions into GFP ($NTD_{MX2}$) demonstrated that phosphorylation at these serines completely prevents the NTD's interaction with HIV-1 CA (Fig. 5a), an attribute that is necessary for MX2 antiviral function[27,28]. As additional confirmation of the requirement for an unphosphorylated NTD

for interacting with CA, GFP ($NTD_{MX2}$) expressed in control cell lysates interacted with CANC assemblies, but failed to do so when expressed in cells depleted of PPP1CB (Fig. 5b).

### MX2 and nuclear import of karyophilic cargo

MX2 accumulates substantially at the nuclear envelope and nuclear pore complexes due to the presence of a targeting signal located within the amino-terminal 25 amino acids[4,27,40], and this has been proposed to be important for the suppression of HIV-1 nuclear import[4,25]. We therefore asked whether phosphorylation of serines 14, 17 and 18 affected the sub-cellular localization of MX2. Indeed, using HeLa cells stably expressing MX2, we found that S14, 17-18D triple mutation significantly reduced MX2 localization at the nuclear envelope, as quantified here as percentage of protein colocalizing (Manders' coefficient) with the nuclear pore complex component NUP358/RanBP2 (Fig. 5c).

It has been recently shown that MX2 interferes with the functionality of different non-viral nuclear localization signals (NLS)[26]. To test the importance of phosphorylation at residues 14, 17 and 18 for this activity, we used a set of ten different GFP-LacZ chimeric proteins tagged at the amino-terminus with different NLSs and observed their nuclear accumulation in HeLa cells expressing MX1, MX2 or the S14, 17-18D mutant. Of these, the nuclear localization of hnRNP K (KNS)-GFP-LacZ was significantly more pronounced in cells expressing the S14, 17-18D mutant compared to the wild type, indicating that phosphorylation at these positions impedes MX2's ability to suppress the nuclear transport of cellular cargo (Fig. 6a, b).

We recently reported that MX2 interacts with the nuclear pore protein NUP214 and the import receptor TNPO1, and that these interactions are important for MX2 antiviral activity[25]. We therefore evaluated the interaction of MX2 S14, 17-18D with both proteins by co-immunoprecipitation, and found that the presence of non-phosphorylated residues at these positions is essential for binding to both NUP214 and TNPO1 (Fig. 6c).

### IFN modulates MX2 NTD phosphorylation

Finally, we investigated whether IFN regulates phosphorylation of the S14-S17-S18 motif. U87-MG $CD4^+$ $CXCR4^+$ cells expressing Flag-tagged MX2 were treated with IFN for 24 h, and the level of phosphorylated MX2 analyzed by immunoblot using anti-P-NTD and anti-Flag antibodies. Strikingly, phosphorylation at the triple-serine motif was substantially reduced in the presence of IFN (Fig. 6d); a similar result was also obtained when analysing a chimeric RFP ($NTD_{MX2}$) protein (Fig. 6e). Based on our data showing that dephosphorylation of these serines is required for MX2 antiviral function, we therefore propose that IFN induces MX2 function through a combination of post-translational and transcriptional mechanisms.

## Discussion

MX2 is one of the main post-entry restriction factors for HIV-1. MX2 accumulates at the nuclear envelope and inhibits viral entry into the nucleus. The NTD, which has a pivotal role in MX2 function, contains a triple-arginine motif that is essential for HIV-1 inhibition and

interaction with the HIV-1 capsid[11,21–23, 27–29,39]. Here, we used SILAC-based interaction screens to identify MYPT1 and PPP1CB as MX2-interacting proteins (Fig. 1). Both proteins are components of MLCP, a member of the PP1 family of cellular phosphatases. We found MLCP is a key regulator of the antiviral activity of MX2. Depletion or pharmacologic inhibition of MLCP reduces the ability of MX2 to inhibit HIV-1, while increasing the level of phosphorylation of serines 14, 17 and 18 within the NTD. Phosphorylation of this serine motif impedes the interaction of the NTD with the viral capsid, while also relieving the MX2-imposed suppression of nuclear import of non-viral karyophilic cargo.

PP1 complexes engage a variety of substrates through multiple binding motifs (reviewed in ref[41]) and are involved in myriad biological processes including muscle contraction, cell division and the regulation of virus replication[31,38,42,43]. The W-P-Y-R-R-R sequence (residues 8 to 13) found in the MX2 NTD represents a good match with one PP1 consensus binding site, and co-immunoprecipitation confirmed that MYTP1 and PPP1CB interact with this sequence (Fig. 1c). Gene silencing experiments demonstrated that depletion of MYPT1 or PPP1CB reduces the antiviral potency of MX2 (Fig. 2a), whereas simultaneous knock-down failed to reduce further antiviral activity supporting our conclusion that MYPT1 or PPP1CB act through a common factor or pathway, namely MLCP.

The role of MLCP in regulating MX2 function was further validated in experiments using established pharmacological inhibitors of protein phosphatases (Fig. 2c). Importantly, parallel analyses using either the MX2-insensitive virus MLV or the HIV-1 CA mutant P90A failed to show any effects on infectivity, demonstrating the selectivity of MLCP action in promoting MX2-mediated inhibition of wild type HIV-1 infection. Because MX2 is an ISG, it was also important to verify the role of MLCP during the IFN-mediated antiviral response. Accordingly, we depleted endogenous MX2 to show that the reductions in the inhibitory effects of IFN that are observed following MLCP silencing or inhibition are reliant on MX2 (Fig. 3a), and confirmed that MLCP is required for the full IFN-induced suppression of HIV-1 in primary $CD4^+$ T cells (Fig. 3c, e).

We turned to mass spectrometry to analyse post-translational modifications of MX2 (Fig. 4). Focusing on the NTD, we found that serine phosphorylation at positions 14, 17 and 18 regulates antiviral function: when unphosphorylated, MX2 is active, but when phosphorylated at these positions MX2 becomes inactive (Fig. 4d). MLCP therefore promotes MX2 antiviral function by maintaining the unphosphorylated state of these serines. Critically, compromising MLCP function displays a consistent relationship with the impairment of MX2's antiviral activity and increased phosphorylation of the S14-S17-S18 motif (Fig. 4d, e, f). That this pattern of regulation of viral inhibition was recapitulated with NTD-containing chimeric proteins ((Extended data Fig. 5a) points to an MX2 regulatory mechanism that is independent of other regions of MX2.

We also examined the consequences of serine phosphorylation for MX2's interactions with known ligands, with compromised binding to HIV-1 capsid (Fig. 5a), NUP214 and TNPO1 (Fig. 6c) being noted, further attesting to the relevance of dephosphorylation at these positions. Consistent with its loss of binding to NUP214/ TNPO1 and reminiscent of

what has been described in cells depleted of both proteins[25], the inactive S14, 17-18D MX2 mutant displays reduced ability to accumulate at the nuclear envelope (Fig. 5c).

Though a complete understanding of the regulation of MX2 by phosphorylation/dephosphorylation will require identification of the relevant kinase(s), we found that IFN treatment substantially reduces phosphorylation at the MX2-triple-serine motif (Fig. 6d, e). This raises the intriguing possibility that NTD phosphorylation is used as a "switch" to inactivate MX2 during basal conditions. Then, in the IFN-induced antiviral state, MX2 is not only induced by transcription, but is also activated via NTD phosphorylation. In support of this model, we examined MX2-mediated inhibition of the nuclear import of non-viral cargo[26] and found that the import efficiency of a representative cellular NLS is impeded less efficiently by the S14, 17-18D mutant than by wild type MX2 (Fig. 6) – put differently, NTD serine phosphorylation limits its capacity to disrupt nucleocytoplasmic trafficking.

Given that a naturally expressed short isoform of MX2 serves as competitive inhibitor of full length MX2[28], thereby providing another mechanism for down-regulating MX2, we conclude that balancing of MX2-mediated innate immunity with the preservation of normal cell function when MX2 is present at basal levels[3] is of fundamental benefit to the host.

## Online Methods

### HIV-1 molecular clones and retroviral vectors

The HIV-1 NL4-3/Nef-IRES-Renilla reporter virus, wild type or P90A HIV-1 based lentiviral particles expressing GFP (HIV-1/GFP), MLV based retroviral particles expressing GFP (MLV/GFP), the pEasiLV inducible and IRES-puromycin N-acetyltransferase (puromycinR) lentiviral vector systems have been described previously[3,13,24,25]. Retroviral based particles expressing GFP-LacZ fusion proteins have been described[26]. Briefly, particles were produced by co-transfection of 293T cells with p5349, pMD.G and the specific GFP-LacZ construct plasmid at a ratio of 1:0.25:1, respectively. In all cases, transfections were performed using TransIT-2020 (Mirus) reagent at a 2:1 ratio with DNA. In all cases, culture medium was changed 24 h after transfection and again after a further 24 h, and filtered through 0.45 μm cut-off filters (Sartorius) to purify viral particles. Resulting media was either used stored at - 80°C for future use (HIV/GFP, MLV/GFP and NL4-3/Nef-IRES-Renilla) or used immediately for transductions (pEasiLV, puromycinR and GFP-LacZ particles).

### Cells

293T cells, HeLa cells and U87-MG cells were obtained from the American Type Culture Collection (ATCC, ATCC® CRL-1573, ATCC® CCL-2 and ATCC® HTB-14 respectively). U87-MG $CD4^+$ $CXCR4^+$ cells, which stably express CD4 and CXCR4 were derived from U87-MG cells and have been described[3]. All cell lines were cultured in Dulbecco's modified Eagle medium (DMEM) supplemented with heat-inactivated foetal bovine serum (10%), L-glutamine, penicillin (100 U/ml) and streptomycin (100 μg/ml). Human primary $CD4^+$ T cells were obtained from peripheral blood mononuclear cells (PBMCs) from healthy volunteer donors (approved by the Guy's Research Ethics Committee (Ref 03/02/06),

and through the Infectious Diseases BioBank at King's College London (ethics reference MM2-220518) under overall permission from the Southampton and South West Hampshire Research Ethics Committee (B) (REC reference 19/SC/0232). $CD4^+$ T cells were isolated from PBMCs using LymphoPrep (Axis-Shield) and the $CD4^+$ T Cell Isolation Kit (Miltenyl Biotec). The purity of isolated cell populations was consistently over 90%, as determined by flow cytometric analysis of specific markers (CD4 and CD3) using anti-CD4 (BD Pharmingen, 555349) and anti-CD3 (BD Pharmingen, (555340) antibodies. Cells were activated by addition of Dynabeads Human T-Activator CD3/CD28 (ThermoFisher) and 50 U/ml recombinant IL-2 (rIL-2) (Roche) for 48 h in Roswell Park Memorial Institute (RPMI) 1640-GlutaMax medium, supplemented with 10% heat-inactivated autologous serum, penicillin (100 U/ml) and streptomycin (100 μg/ml). After activation, $CD4^+$ T cells were further maintained in same medium containing 30 U/ml rIL-2. In some experiments, culture medium was supplemented with 500 or 2,000 U/ml IFNα-2b (INTRON A, Merck, Sharpe & Dohme Corp.).

## siRNA mediated knock-down

Cultures of 50,000 U87-MG $CD4^+$ $CXCR4^+$ based cells were transfected twice, 24 h apart, with 10 nM of either smartpool siRNAs (Dharmacon) (for CTR (D-001210-03-05), MYPT1 (PPP1R12A) (M-011340-01-0005), PPP1CB (M-008685-00-0005) or MX2 (M-011736-01-0005)) or individual siRNAs (for MYPT1 (MQ-011340-01-0002) and PPP1CB (MQ-008685-00-0002)). In cases when IFNα was used, 8 h after the second transfection 500 U/ml IFNα was added to one dish of cells, while a second identical culture was left untreated. 24 h after IFNα addition, cells were challenged with HIV-1/GFP particles, and infectivity measured 48 h later by flow cytometry (FACSCalibur, BD Biosciences, and FlowJo 10.6) (the gating strategy used is displayed in (Extended data Fig. 6). The efficiency of knock-down was examined by immunoblot analysis of whole cell lysates harvested 32 h after the second siRNA transfection using anti-MYPT1 (Abcam, ab70809), anti-PPP1CB (Abcam, ab53315), anti-MX2 (Novus Biologicals, NBP1-81018) and anti-tubulin (Sigma, T5168).

## Plasmids

cDNAs corresponding to MX1, MX2, MX2 R11-13A, GFP or GFP ($NTD_{MX2}$) were inserted into pCTAP-A (Agilent Technologies) to perform stable isotope labelling by amino acids (SILAC) analysis of MX2 interacting proteins. pEasiLV[3] containing luciferase (Luc), wild type MX2, MX2 mutants or chimeric proteins (Fv1b ($NTD_{MX2}$) and MX1 ($NTD_{MX2}$)) were produced by standard cloning or site directed mutagenesis. pEasiLV-BFP was obtained by substitution of the E2 crimson marker for blue fluorescent protein (BFP), and used for the insertion of DNAs encoding Luc, MYPT1 or PPP1CB. Wild type HIV-1 Capsid-Nucleocapsid (CANC, Gag residues 133-432), was cloned into pET-11a plasmid (Adgene). MX1, MX2 and MX2 S14, 17-18D were cloned into the puromycinR lentiviral vector replacing CD4 (Goujon, 2013). Retroviral based vectors expressing GFP-LacZ fusion proteins, as well as derivatives containing nuclear localization sequences (NLSs) for SV40 large T antigen, c-MYC, DDX21, *Xenopus laevis* NUPL, HnRNP K (KNS), HTLV-1 Rex or residues 1 to 25 of MX2 (NMX2) were based on the retroviral LHCX vector and were kindly provided by Paul Bieniasz and Melissa Kane. Mutants NLS (NMX2) S14, 17-18A-

GFP-LacZ and NLS (NMX2) S14, 17-18D-GFP-LacZ were obtained by site directed mutagenesis. pCAGGS vectors encoding Flag- or HA-tagged GFP, GFP ($NTD_{MX2}$), MX1, MX1 ($NTD_{MX2}$), MX2, C-terminal fragment (residues 1681-2080) of NUP214, TNPO1 or mutant derivatives have been described[21,24,25].

## CRISPR-Cas9 knock-out cells

Control CRISPR U87-MG $CD4^+$ $CXCR4^+$ cells and MX2 CRISPR_1 clone have been described[25]. MX2 CRISPR U87-MG $CD4^+$ $CXCR4^+$ bulk cells, as well as MX2 CRISPR_2 clone were generated using different specific guide RNAs targeting *MX2* cloned into BsmBI-linearized lentiviral vector pLentiCRISPRv2[44,45] using the oligonucleotides (forward/reverse) 5'-caccgGACAACCAGCCCCGAGACAT-3' and 5'-aaacATGTCTCGGGGCTGGTTGTCc-3'. Retroviral vectors expressing the guides were produced in 293T cells by transfection of HIV-1 packaging plasmid p8.91, vesicular stomatitis virus G (VSV-G) envelope vector (pMD.G) and pLentiCRISPRv2 at a ratio of 1.5:0.375:1.5, respectively. After transduction, U87-MG $CD4^+$ $CXCR4^+$ cells were selected for 72 h in the presence of 1 μg/ml puromycin (Sigma). Single clone MX2 CRISPR_2 was derived from the bulk population by single-cell sorting in 96-well plates and the loss of MX2 confirmed by immunoblotting. *MX2* gene disruption was validated by sequencing of the targeted genomic region (Genewiz).

## shRNA-mediated silencing

$CD4^+$ T cell gene silencing was achieved using a modified version of the HIV-1 based lentiviral vector pHRSIREN-S-SBP-ΔLNGFR-W where the antibody-free magnetic cell sorting selectable marker (SBP-ΔLNGFR) was replaced by E2-crimson[9,25]. The shRNA targeting sequences for the negative control (scramble), MX2, PPP1CB and MYPT1, were 5'-GTTATAGGCTCGCAAAAGG-3', 5'-AAGATGTTCTTTCTAATTG-3', 5'-AGATTTGATTTGTCGAGCT-3' and 5'-GATGAAGAGTCTGAATCCC-3', respectively. Lentiviral vector stocks were obtained by co-transfection of 293T cells with pMD.G, p8.91 and pHRSIREN vector at a ratio of 0.5:1:1.5. After filtration, cell culture supernatants containing lentiviral particles were concentrated by ultracentrifugation at 28,000 x g for 75 min. Human primary $CD4^+$ T cells were then transduced by spin-infection at 2,000 x g for 2 h at room temperature. Two days later, 3 x $10^4$ cells/well were seeded in 96 well plates in duplicates. 2,000 U/ml of IFNα was added to one of the wells, while the other was left untreated. 24 h later, cells were challenged with NL4.3/Nef-IRES-Renilla (measured as 30 ng $p24^{Gag}$) at 2,000 x g for 2 h at room temperature. Infection was left to proceed for 48 h, and infectivity levels were assessed by measuring Renilla luciferase activity using the Renilla Luciferase Assay System (Promega).

## Quantification of mRNA expression

~$10^6$ activated primary human $CD4^+$ T cells treated or not for 24 h with 2,000 U/ml IFNα were collected and the RNA was extracted using the RNeasy Mini Kit (Qiagen). cDNA was produced using 500 ng of purified RNA and the High-Capacity cDNA Reverse Transcription Kit (Thermo Fisher). Quantitative PCR (qPCR) of selected genes was then performed using the following TaqMan gene expression assays (Thermo Fisher): MYPT1 (Hs01552899),

PPP1CB (Hs01027793), MX2 (Hs01550808) and GAPDH (Hs99999905). GAPDH was used to normalized expression levels.

### Stable isotope labelling by amino acids (SILAC)

293T cells were grown in DMEM with no glutamine, no lysine, and no arginine (Thermo Fisher) supplemented with 10% dialyzed fetal bovine serum, 6 mM L-glutamine, 100 U/ml penicillin, 100 μg/ml streptomycin, containing either: a) 73 mg/l $^{13}C_6$ $^{15}N_2$-L-lysine (Lys8) and 42 mg/l $^{13}C_6$ $^{15}N_4$-L-arginine (Arg10) (CK Isotopes) for “heavy” conditions; b) 73 mg/l 4,4,5,5-D4-L-Lysine (Lys4) and 42 mg/l $^{13}C_6$-L-arginine HCl (Arg6) (CK Isotopes) for “medium” conditions; c) 73 mg/l L-lysine (Lys0) and 42 mg/l L-arginine (Arg0) (Sigma) for “light” conditions. Cells were grown on the aforementioned media for at least two weeks prior to their use.

### MX2 interacting proteins and mass spectrometry

For the identification of MX2 interacting proteins, groups of five 15 cm dishes of 293T cells variously labelled with “light”, “medium” or “heavy” arginine and lysine amino acids were transfected with 20 μg/dish of pCTAP-A vectors expressing either MX1, MX2, MX2 R11-13A, GFP or GFP ($NTD_{MX2}$), or empty vector. At 48 h, cells were lysed and over-expressed proteins isolated by streptavidin-affinity purification using the InterPlay Mammalian TAP System (Agilent Technologies). Samples obtained from “light”, “medium” and “heavy” conditions were pooled together and resolved using 12% SDS-polyacrylamide gels and stained with SimplyBlue (Thermo Fisher). In-gel reduction, alkylation and trypsin digestion were subsequently conducted. Peptides were extracted from the gel by a series of washes of acetonitrile and water and subsequently lyophilised. Resulting samples were resuspended in 50 mM $NH_4HCO_3$ and analyzed by LC-MS/MS. Chromatographic separations were performed using an EASY nLC-II nanoflow system (Thermo Fisher). Reversed phase chromatography was used to resolve peptides, using a 75 μm C18 PepMap column and three step linear gradient of acetonitrile in $CH_2O_2$ (0.1%) at 300 nl/min. The eluate was ionised by electrospray ionisation using an Orbitrap Velos Pro (Thermo Fisher, UK) operating under Xcalibur v2.2. The instrument was programmed to acquire in automated data-dependent switching mode, selecting precursor ions based on their intensity for sequencing by collision-induced fragmentation using a Top20 CID method. The MS/MS analyses were performed using collision energy profiles that were selected based on the mass-to-charge ratio (m/z) and the charge state of the peptide. Database searching was carried out using MaxQuant v1.4.3.14 (Max Planck Institute of Biochemistry) against the Uniprot human database (https://www.uniprot.org/proteomes/UP000005640). Parameters for single protein identification were set including cysteine carbamidomethylation as a fixed modification, with N-terminus acetylation and methionine oxidation as variable modifications. The minimum peptide length allowed was 7 and a maximum number of modifications per peptide of 5. Peptide-spectrum-matches and proteins were retained if they were below a false discovery rate of 1%. Additional analyses were conducted using Perseus software (version 1.4.1.3), obtaining sample relative abundancy of identified proteins after removal of potential contaminants and reverse proteins. Illustrative pairwise comparisons are shown in Fig. 1a, though additional comparisons using different labels for the same protein pairs yielded similar results.

In experiments performed to study specific sites of MX2 phosphorylation, Flag-tagged immunoprecipitated protein samples from 293T cell lysates were reduced, alkylated and digested in-gel using Lys-C endoproteinase. The resulting peptides were re-suspended in 20 μl sample solution (3% MeCN, 0.1% trifluroacetic acid) and LC-MSMS data acquisition was performed on an Orbitrap Fusion Lumos (ThermoFisher) coupled to an RSLC3000 nanoHPLCs (ThermoFisher). The Fusion Lumos was configured with an EASYspray source using a 50 cm PepMap EASYspray emitter at 40°C. The nanoHPLC was operated with solvent A (0.1% $CH_2O_2$) and solvent B (80% MeCN, 0.1% $CH_2O_2$) at 250 nl/min with peptides resolved using a gradient rising from 3 to 40% solvent B by 60 min. MS data were acquired at 120k resolution between m/z 375 and 1500 with an AGC target of 4.0e5. MS2 isolation was performed in the quadrupole with HCD activation and 30% collision energy with fragment ions scanned in the Orbitrap at 30k resolution.

Data were processed in PEAKS 8 (Bioinformatics Solutions Inc., Ontario). A precursor mass error tolerance of 4.0 ppm and a fragment ion tolerance of 0.02 Da was used with a Uniprot Human database (https://www.uniprot.org/proteomes/UP000005640, downloaded 15/01/19), with the search performed using the default 485 built-in modifications.

## Immunoprecipitation

Co-immunoprecipitations were conducted to confirm interactions between MX2 and endogenous PPP1CB or MYPT1, or ectopically expressed C-terminal fragment of NUP214 or TNPO1. 293T cells were seeded in 6-well plates and transfected singly with pCAGGs vectors expressing triple-HA tagged MX1, MX2 or MX2 R11-13A, or co-transfected with vectors expressing triple-HA tagged MX1, MX2 or MX2 S14, 17-18D and either pCAGGs vectors expressing Flag-tagged C-terminal fragment of NUP214 or TNPO1. At 48 h, cells were collected in lysis buffer (1x phosphate buffered saline, 0.5% Triton-X100, 1x complete protease inhibitor cocktail (Roche)) and lysed by sonication for 20 s. After lysate clarification for 10 min at 1500 x g and 4°C, a sample was withdrawn for analysis as input. Cell lysates were incubated with anti-HA magnetic beads (Pierce) for 2 h at 4°C. Beads were then washed with lysis buffer 4 times before resuspension in sample buffer (200 mM Tris-HCl pH 6.8, 5.2% SDS, 20% glycerol, 0.1% bromophenol blue, 5% β-mercaptoethanol). HA- and Flag-tagged proteins were resolved using 12% SDS-polyacrylamide gels and detected by immunoblotting using anti-HA (Sigma, 12013819001) and anti-Flag (Sigma, A8592) antibodies.

To determine the phosphorylated residues in MX2, ten 15 cm dishes of 293T cells stably expressing Flag-tagged MX2 were obtained by transduction with puromycinR lentiviral vector and selection with 1.5 μg/ml of puromycin for 72 h. Cells were lysed in lysis buffer from the InterPlay Mammalian TAP System (Agilent Technologies), supplemented with 1x PhosSTOP phosphatase inhibitor cocktail (Sigma) and 1x complete protease inhibitor cocktail (Roche). The resulting lysate was cleared by centrifugation at 16,000 x g for 10 min, and the supernatant was incubated with anti-Flag magnetic beads for 2 h at 4°C. The beads were washed 3 times with lysis buffer, resuspended in sample buffer and boiled for 10 min. Immunoprecipitated MX2 was resolved on a pre-cast 12% SDS-polyacrylamide gel

(Thermo Fisher), stained with SimplyBlue (Thermo Fisher) and the band corresponding to MX2 excised for MS/MS analysis (see above).

### Anti-phospho (P)-NTD MX2 antiserum production

The anti-P-NTD MX2 antiserum (AB2978) was generated using rabbits and a custom antibody production service (Thermofisher). Sera were harvested 124 days after initial immunization with the C-PYRRR(pS)QF(pS)(pS)RK-amide peptide corresponding to amino acids 9 to 20 of MX2. The animals received four immunization boosts.

### Immunoblotting

Cells were lysed in buffer containing 10 mM Tris-HCl pH 8, 150 mM NaCl, 1 mM EDTA, 1% Triton X-100 and 0.1% sodium deoxycholate. Lysates were briefly sonicated, boiled for 10 min and resolved in 12% SDS-polyacrylamide gels. After electrophoretically transferring proteins to a 0.45 μm nitrocellulose membrane (Amersham), their presence was analyzed using specific antibodies.

### Immunofluorescence microscopy

HeLa cells stably expressing Flag-tagged wild type or mutant MX2 proteins, or MX1, were obtained by transduction with puromycinR lentiviral particles encoding the appropriate DNA and selection with 1 μg/ml puromycin for 72 h. Stable cells were seeded onto coverslips at ~20,000 cells per well in 24-well plates. At 24 h, cells were washed three times with 1x phosphate buffer saline (PBS) and fixed in 4% paraformaldehyde (EM Sciences) for 15 min, before permeabilization with 0.2% Triton X-100 for 15 min. The specimens were blocked in buffer NGB (50 mM $NH_4Cl$, 2% goat serum, 2% bovine serum albumin) for 1 h. Flag-tagged proteins were detected using a mouse anti-Flag monoclonal M2 (Sigma, F3165) and secondary donkey anti-mouse antibody conjugated to Alexa 594 (Invitrogen, A-21203). Endogenous NUP358 was detected using rabbit anti-NUP358 polyclonal antibody (Abcam, ab64276) and secondary donkey anti-rabbit antibody conjugated to Alexa 488 (Invitrogen, A-21206). DAPI (4’,6-diamidino- 2-phenylindole) staining was used to demarcate the nucleus (0.1 mg/ml for 5 min).

Experiments conducted to address the behaviour of GFP-LacZ proteins bearing different NLSs have been described[26]. Briefly, retroviral LHCX-based vectors containing different NLS-GFP-LacZ constructs were used to transduce HeLa cells. At 48 h, 600 μg/ml hygromycin (Invitrogen) was added for 5 days and hygromycin-resistant cells further transduced with puromycinR lentiviral particles expressing Flag-tagged MX1, MX2 or MX2 S14, 17-18D. 48 h later, puromycin-resistant cells were selected as described above, seeded on coverslips and subjected to immuno-staining. Cells were visualized using a Nikon A1 point-scanning laser confocal microscope (Nikon Instruments). Images were analyzed with ImageJ Fiji and the JACoP tool (Boltec and Cordelières, 2006). Quantification of the nuclear localization of wild type MX2 and MX2 S14, 17-18D was calculated as the percentage of total protein colocalizing with NUP358, using Manders’ coefficient. In the case of the extent of nuclear localization of KNS-GFP-LacZ Manders’ coefficient was used to quantify the colocalization with DAPI stain.

Europe PMC Funders Author Manuscripts

## Drugs

Protein phosphatase inhibitors calyculin A (Abcam), okadaic acid (Enzo) and rubratoxin A (Abcam) were dissolved in DMSO. In all infectivity experiments, cells were treated with the desired drug concentration 6 h before infection (or DMSO as a negative control), and medium was changed 24 h after treatment.

## CANC pull-down assays

CANC protein was expressed in *Escherichia coli* Rosetta (DE3) cells (Merck Millipore) as previously described[47]. Assembled CANC complexes were prepared by dilution of the protein to 40 μM final concentration in 50 mM Tris-HCl pH 8 containing 100 mM NaCl and adding 5 μM of TG50 oligonucleotide (5'- $TG_{(25)}$-3'). The reaction was incubated overnight at room temperature. For pull-down experiments, protein over-expression was achieved by transient transfection of 293T cells with relevant vectors. When used, siRNAs were transfected doubly, 24 h apart at a concentration of 10 nM. At 48 h after transfection, cells were lysed in hypotonic lysis buffer (10 mM Tris-HCl pH 8, 10 mM KCl, 1x complete protease inhibitor cocktail [Roche]) using a Dounce homogeneizer. Cell lysates were cleared by centrifugation at 20,000 x g for 15 min at 4°C. 200 μl of the lysate was mixed with either 40 μl of Capsid assembly buffer (Cab, 50 mM Tris-HCl pH 8, 100 mM NaCl) containing 5 μM TG50 (as a control), or with 40 μl 40 μM of assembled CANC; an input sample was withdrawn from the latter. The mixtures were incubated for 1 h at room temperature, prior to overlay on a 250 μl 70% sucrose cushion. Following centrifugation at 20,000 x g for 15 min at room temperature, a sample of the resulting supernatant was withdrawn, and the pellet washed with 500 μl of wash buffer (50 mM Tris-HCl pH 8, 50 mM NaCl and 5 mM KCl), and re-pelleted at 10,000 x g for 8 min. Finally, washed pellet was resuspended in 50 μl sample buffer. Input, supernatant and pellet fractions were analyzed by immunoblotting using anti-CA[48] and anti-Flag (Sigma, A8592) antibodies.

## Quantification and statistical analysis

Statistical parameters in charts are expressed as means ± standard deviation (sd) for experimental replicates in each case, including the exact number of n. Differences between the experimental groups were evaluated, where indicated, by paired or unpaired two-tailed t-tests. Statistical significance in figures are denoted by asterisks (*$p < 0.05$, ns = not significant).

In experiments analysing protein abundancy by immunoblot, band intensities were quantified using Image J v1.51u software. Statistical analysis was performed in GraphPad PRISM 6 (Graph Pad software).

Europe PMC Funders Author Manuscripts

## Extended Data

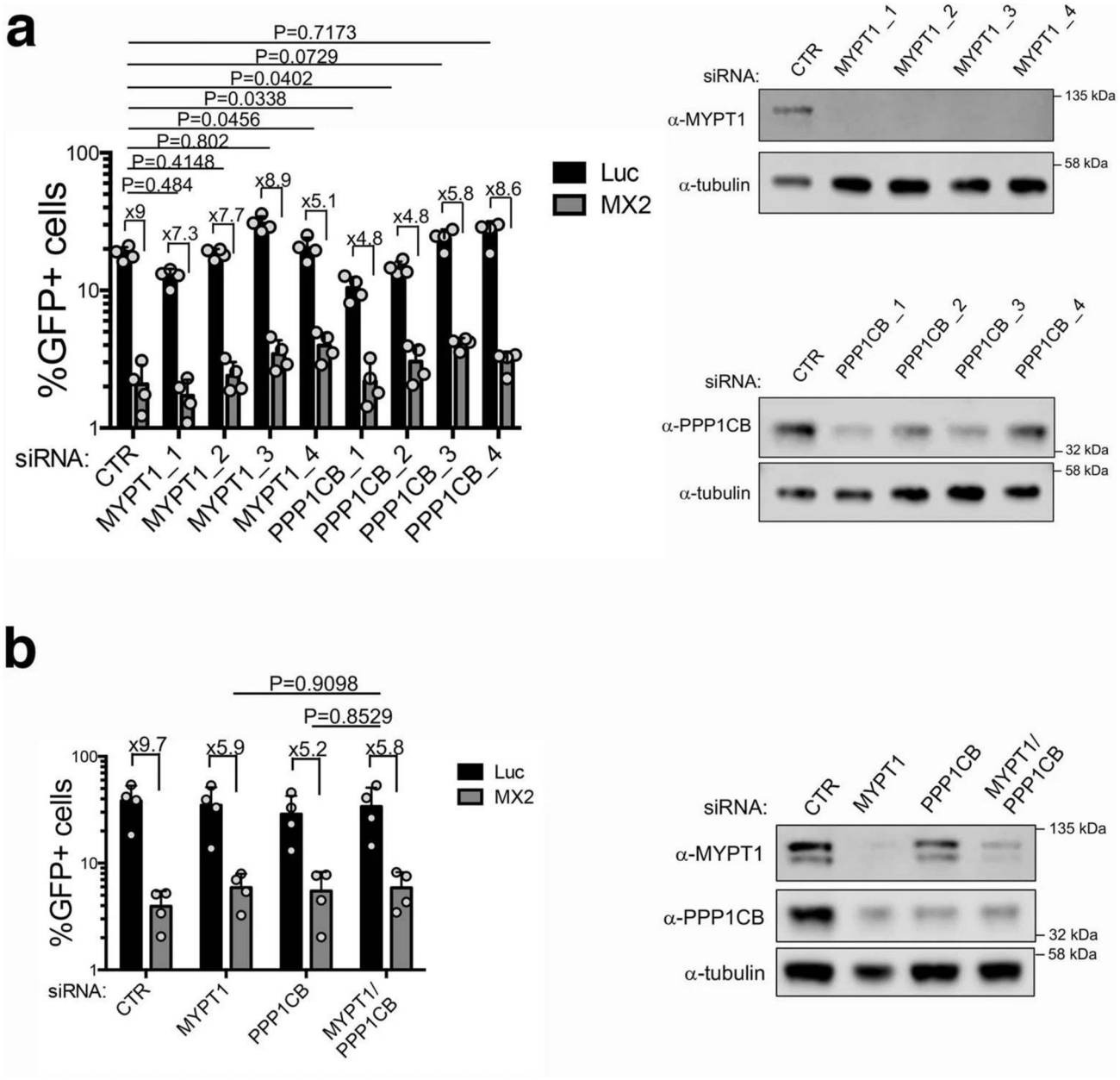


**Extended Data Fig. 1.**

Europe PMC Funders Author Manuscripts

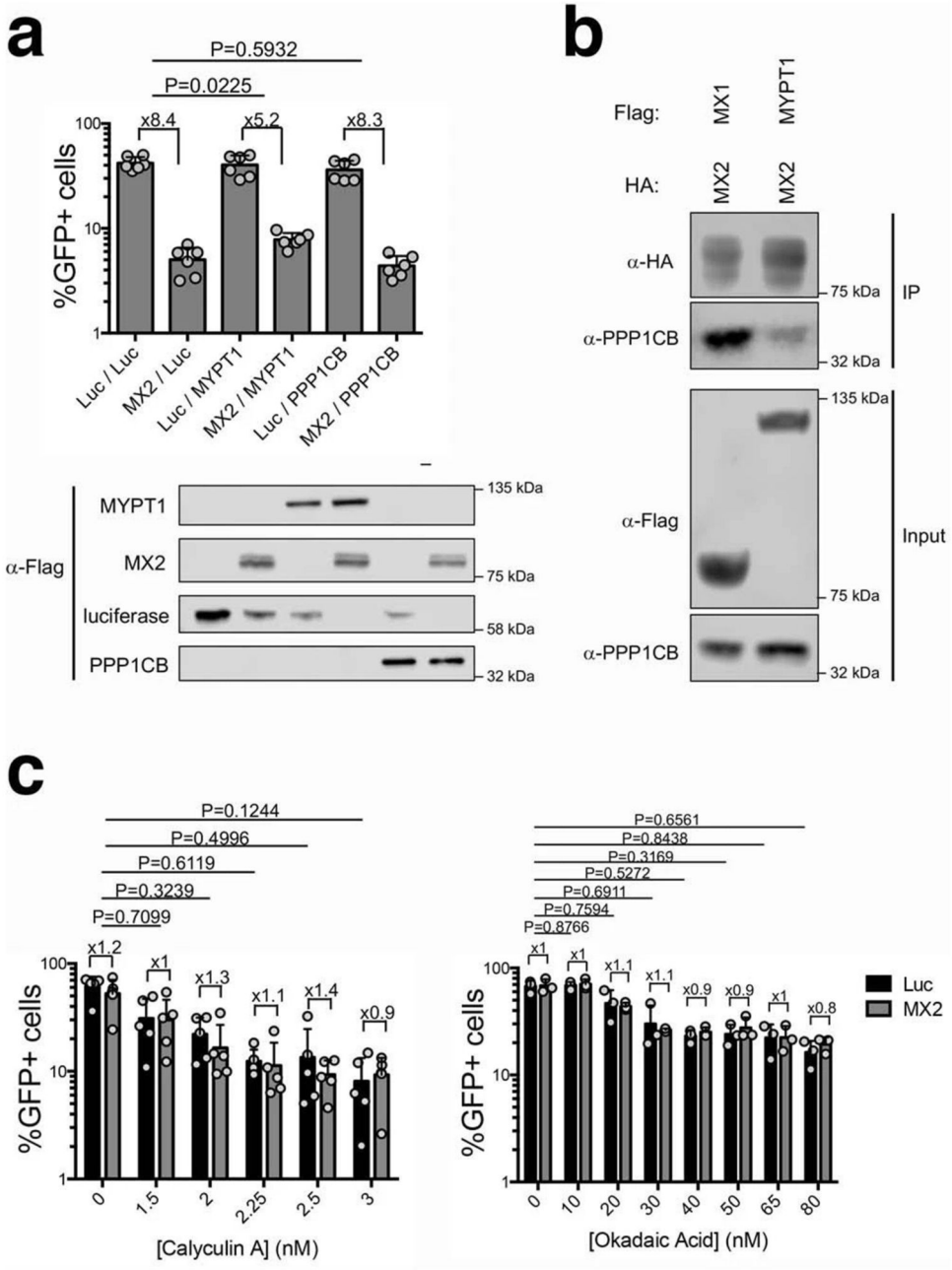


**Extended Data Fig. 2.**

Europe PMC Funders Author Manuscripts

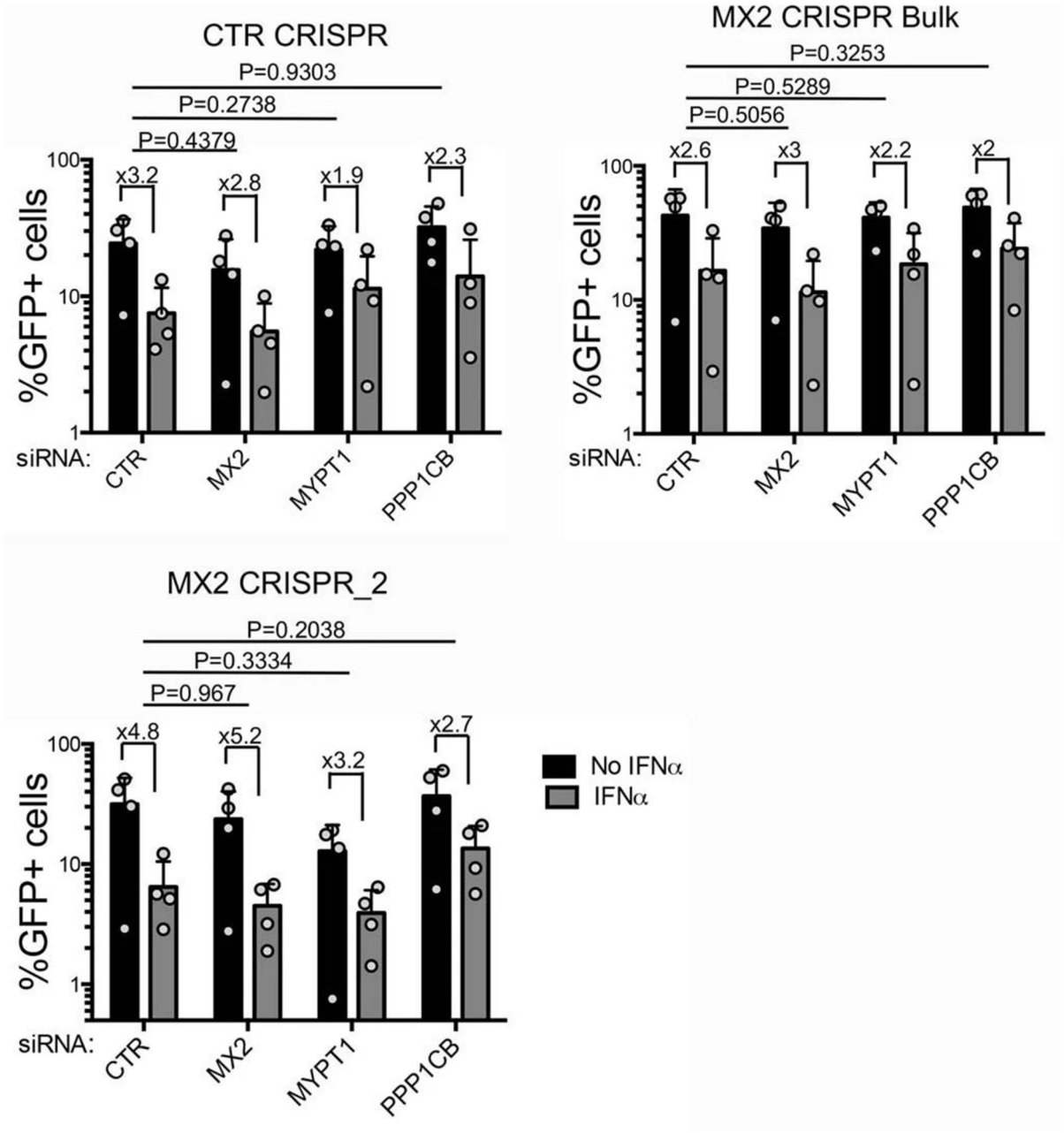


**Extended Data Fig. 3.**

Europe PMC Funders Author Manuscripts

**a**

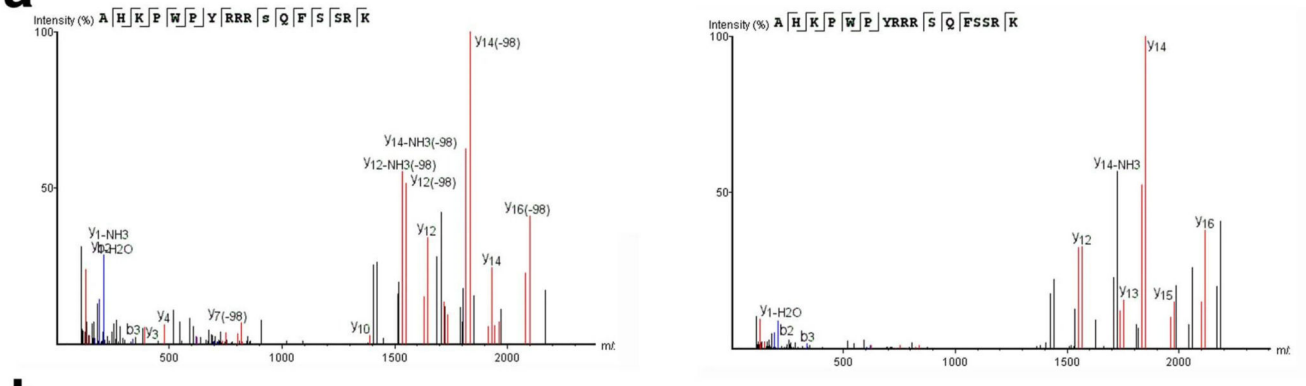


**b**

| | Peak area |
|---|---|
| Unmodified | 2.55 $e^8$ |
| $^P$S14 | 1.16 $e^9$ |
| $^P$S17 | 2.04 $e^8$ |
| $^P$S18 | 4.32 $e^8$ |

**Extended Data Fig. 4.**

Europe PMC Funders Author Manuscripts

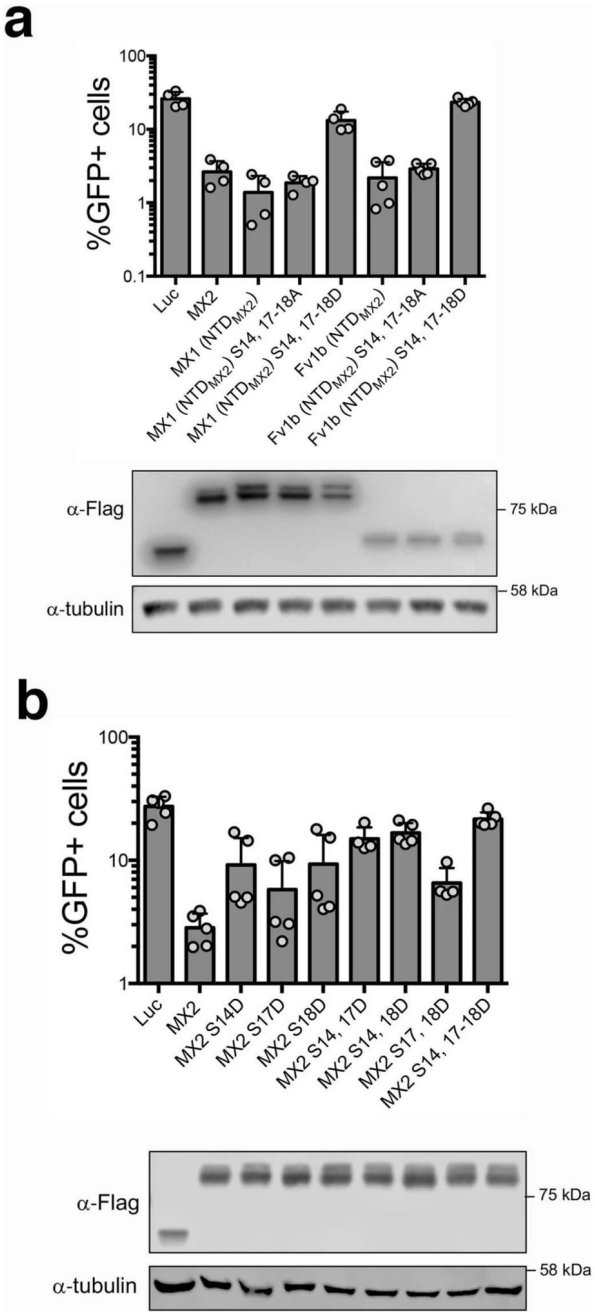


**Extended Data Fig. 5.**

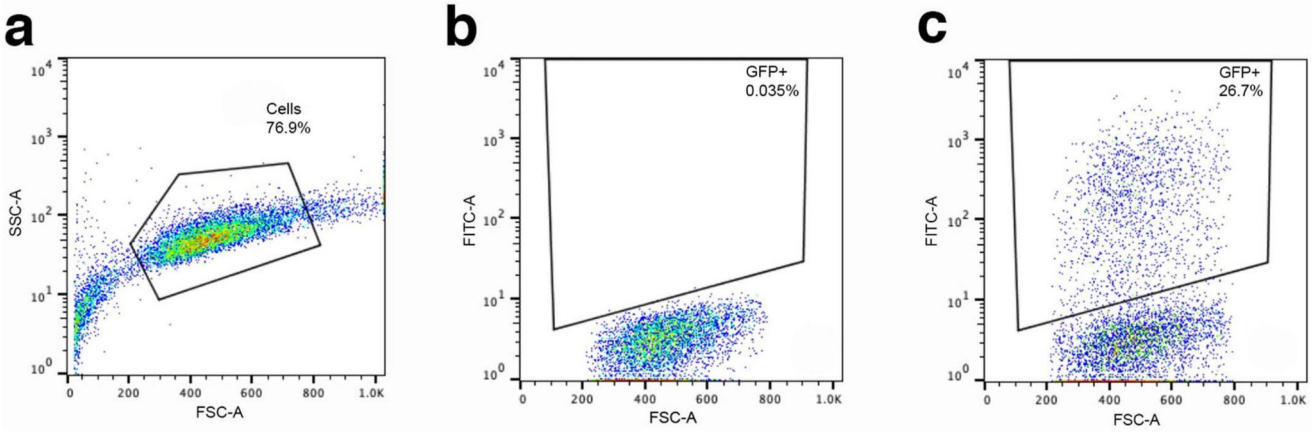


**Extended Data Fig. 6.**

## Acknowledgments

We thank Darja Pollpeter, Leandro Ventimiglia, Stelios Papaioannou, Paul Lehner, John Cason, Christine Mant, Melissa Kane and Paul Bieniasz for the provision of reagents and helpful discussions. The work was supported by the Wellcome Trust (106223/Z/14/Z), the Medical Research Council (MR/M001199/1), the National Institutes of Health (U54 GM103368, AI150472) and the Department of Health via a National Institute for Health Research comprehensive Biomedical Research Centre award to Guy's and St. Thomas' NHS Foundation Trust in partnership with King's College London and King's College Hospital NHS Foundation Trust. J.M.J.-G. is a Long-Term Fellow of the European Molecular Biology Organization (EMBO) (ALTF 663-2016).

## Data availability

For further information and requests for reagents, please contact the Lead Contact, Michael H. Malim (michael.malim@kcl.ac.uk). The plasmids generated in this study are available upon request without restriction. All datasets generated in this study are available as source data. The mass spectrometry proteomics data have been deposited to the ProteomeXchange Consortium via the PRIDE[49] partner repository with the dataset identifier PXD026073 (SILAC data) and PXD026090 and 10.6019/PXD026090 (phosphorylation data).

## Data and code availability

This study did not generate any unique datasets or code.

## References

1. Doyle T, Goujon C, Malim MH. HIV-1 and interferons: who's interfering with whom? Nature Reviews Microbiology. 2015; 13 :403–403. [PubMed: 25915633]
2. Bourke NM, et al. Control of HIV infection by IFN-α: implications for latency and a cure. Cellular and Molecular Life Sciences. 2018; 75 :775–783. [PubMed: 28988399]
3. Goujon C, et al. Human MX2 is an interferon-induced post-entry inhibitor of HIV-1 infection. Nature. 2013; 502 :559–562. [PubMed: 24048477]
4. Kane M, et al. MX2 is an interferon-induced inhibitor of HIV-1 infection. Nature. 2013; 502 :563–566. [PubMed: 24121441]
5. Liu Z, et al. The interferon-inducible MxB protein inhibits HIV-1 infection. Cell Host Microbe. 2013; 14 :398–410. [PubMed: 24055605]

6. Crameri M, et al. MxB is an interferon-induced restriction factor of human herpesviruses. Nat Commun. 2018; 9 :1980. [PubMed: 29773792]
7. Schilling M, et al. Human MxB protein is a pan-herpesvirus restriction factor. J Virol. 2018; 92 :17.
8. Staeheli P, Haller O. Human MX2/MxB: a Potent Interferon-Induced Postentry Inhibitor of Herpesviruses and HIV-1. Journal of Virology. 2018; 92 :24.
9. Jimenez-Guardeño JM, Apolonia L, Betancor G, Malim MH. Immunoproteasome activation enables human TRIM5α restriction of HIV-1. Nature Microbiology. 2019
10. Wang YX, et al. Interferon-inducible MX2 is a host restriction factor of hepatitis B virus replication. J Hepatol. 2019
11. Matreyek KA, et al. Host and viral determinants for MxB restriction of HIV-1 infection. Retrovirology. 2014; 11 :90. [PubMed: 25348155]
12. Busnadiego I, et al. Host and Viral Determinants of Mx2 Antiretroviral Activity. Journal of Virology. 2014; 88 :7738–7752. [PubMed: 24760893]
13. Bulli L, et al. Complex Interplay between HIV-1 Capsid and MX2-Independent Alpha Interferon-Induced Antiviral Factors. J Virol. 2016; 90 :7469–7480. [PubMed: 27279606]
14. Staeheli P, Haller O, Boll W, Lindenmann J, Weissmann C. Mx protein: Constitutive expression in 3T3 cells transformed with cloned Mx cDNA confers selective resistance to influenza virus. Cell. 1986; 44 :147–158. [PubMed: 3000619]
15. Gordien E, et al. Inhibition of Hepatitis B Virus Replication by the Interferon-Inducible MxA Protein. Journal of Virology. 2002; 75 :2684–2691.
16. Haller O, Kochs G. Human MxA Protein: An Interferon-Induced Dynamin-Like GTPase with Broad Antiviral Activity. Journal of Interferon & Cytokine Research. 2010; 31 :79–87. [PubMed: 21166595]
17. Turan K, et al. Nuclear MxA proteins form a complex with influenza virus NP and inhibit the transcription of the engineered influenza virus genome. Nucleic Acids Research. 2004; 32 :643–652. [PubMed: 14752052]
18. Mitchell PS, et al. Evolution-guided identification of antiviral specificity determinants in the broadly acting interferon-induced innate immunity factor MxA. Cell Host Microbe. 2012; 12 :598–604. [PubMed: 23084925]
19. Mänz B, et al. Pandemic Influenza A Viruses Escape from Restriction by Human MxA through Adaptive Mutations in the Nucleoprotein. PLoS Pathogens. 2013; 9 :3.
20. Patzina C, Haller O, Kochs G. Structural requirements for the antiviral activity of the human MxA protein against Thogoto and influenza A virus. Journal of Biological Chemistry. 2014; 289 :6020–6027.
21. Goujon C, et al. Transfer of the Amino-Terminal Nuclear Envelope Targeting Domain of Human MX2 Converts MX1 into an HIV-1 Resistance Factor. Journal of Virology. 2014; 88 :9017–9026. [PubMed: 24899177]
22. Fricke T, et al. MxB binds to the HIV-1 core and prevents the uncoating process of HIV-1. Retrovirology. 2014; 11 :68–68. [PubMed: 25123063]
23. Goujon C, Greenbury RA, Papaioannou S, Doyle T, Malim MH. A Triple-Arginine Motif in the Amino-Terminal Domain and Oligomerization Are Required for HIV-1 Inhibition by Human MX2. Journal of Virology. 2015; 89 :4676–4680. [PubMed: 25673704]
24. Dicks MDJ, et al. Oligomerization Requirements for MX2-Mediated Suppression of HIV-1 Infection. Journal of Virology. 2015; 90
25. Dicks MDJ, et al. Multiple components of the nuclear pore complex interact with the amino-terminus of MX2 to facilitate HIV-1 restriction. PLoS Pathogens. 2018; 14 :1–24.
26. Kane M, et al. Nuclear pore heterogeneity influences HIV-1 infection and the antiviral activity of MX2. eLife. 2018; 7 :1–44.
27. Schulte B, et al. Restriction of HIV-1 Requires the N-Terminal Region of MxB as a Capsid-Binding Motif but Not as a Nuclear Localization Signal. J Virol. 2015; 89 :8599–8610. [PubMed: 26063425]

28. Betancor G, et al. The GTPase Domain of MX2 Interacts with the HIV-1 Capsid, Enabling Its Short Isoform to Moderate Antiviral Restriction. Cell Rep. 2019; 29 :1923–1933. [PubMed: 31722207]
29. Smaga SS, et al. MxB Restricts HIV-1 by Targeting the Tri-hexamer Interface of the Viral Capsid. Structure. 2019; 27 :1234–1245. [PubMed: 31155311]
30. Buffone C, Schulte B, Opp S, Diaz-Griffero F. Contribution of MxB oligomerization to HIV-1 capsid binding and restriction. J Virol. 2015; 89 :3285–3294. [PubMed: 25568212]
31. Kiss A, Erdődi F, Lontay B. Myosin phosphatase: Unexpected functions of a long-known enzyme. BBA-Molecular Cell Research. 2019; 1866 :2–15. [PubMed: 30076859]
32. Heroes E, et al. The PP1 binding code: A molecular-lego strategy that governs specificity. FEBS Journal. 2013; 280 :584–595.
33. Wies E, et al. Dephosphorylation of the RNA Sensors RIG-I and MDA5 by the Phosphatase PP1 Is Essential for Innate Immune Signaling. Immunity. 2013; 38 :437–449. [PubMed: 23499489]
34. Ishihara H, et al. Calyculin A and okadaic acid: Inhibitors of protein phosphatase activity. Biochemical and Biophysical Research Communications. 1989; 159 :871–877. [PubMed: 2539153]
35. Takai A, et al. Inhibitory effect of okadaic acid derivatives on protein phosphatases A study on structure-affinity relationship. Biochemical Journal. 2015; 284 :539–544.
36. Ammosova T, et al. Nuclear targeting of protein phosphatase-1 by HIV-1 Tat protein. Journal of Biological Chemistry. 2005; 280 :36364–36371.
37. Wada SI, et al. Rubratoxin A specifically and potently inhibits protein phosphatase 2A and suppresses cancer metastasis. Cancer Science. 2010; 101 :743–750. [PubMed: 20028386]
38. Takai A, et al. Protein phosphatases 1 and 2A and their naturally occurring inhibitors: current topics in smooth muscle physiology and chemical biology. J Physiol Sci. 2018; 68 :1–17. [PubMed: 28681362]
39. Fribourgh JL, et al. Structural insight into HIV-1 restriction by MxB. Cell Host and Microbe. 2014; 16 :627–638. [PubMed: 25312384]
40. Melén K, et al. Human MxB protein, an interferon-a-inducible GTPase, contains a nuclear targeting signal and is localized in the heterochromatin region beneath the nuclear envelope. Journal of Biological Chemistry. 1996; 271 :23478–23486.
41. Roy J, Cyert MS. Cracking the Phosphatase Code- Docking Interactions Determine Substrate Specificity. Science Signaling. 2009; 2 :100.
42. Grassie ME, Moffat LD, Walsh MP, MacDonald JA. A regulated mechanism for achieving substrate specificity of the catalytic subunit of protein phosphatase type 1δ. Archives of Biochemistry and Biophysics. 2011; 510 :147–159. [PubMed: 21291858]
43. Matsumura F, Yamakita Y, Yamashiro S. Myosin light chain kinases and phosphatase in mitosis and cytokinesis. Archives of Biochemistry and Biophysics. 2011; 510 :76–82. [PubMed: 21396909]
44. Sanjana NE, Shalem O, Zhang F. Improved vectors and genome-wide libraries for CRISPR screening. Nature Methods. 2014; 11 :783–784. [PubMed: 25075903]
45. Shalem O, et al. Genome-scale CRISPR-Cas9 knockout screening in human cells. Science. 2014; 343 :84–87. [PubMed: 24336571]
46. Bolte S, Cordelières FP. A guided tour into subcellular colocalization analysis in light microscopy. Journal of Microscopy. 2006; 224 :213–232. [PubMed: 17210054]
47. Schaller T, et al. Effects of Inner Nuclear Membrane Proteins SUN1/UNC-84A and SUN2/UNC-84B on the Early Steps of HIV-1 Infection. J Virol. 2017; 91 :19.
48. Fouchier RA, Meyer BE, Simon JH, Fischer U, Malim MH. HIV-1 infection of non-dividing cells: evidence that the amino-terminal basic region of the viral matrix protein is important for Gag processing but not for post-entry nuclear import. EMBO J. 1997; 16 :4531–4539. [PubMed: 9303297]
49. Perez-Riverol Y, et al. The PRIDE database and related tools and resources in 2019: improving support for quantification data. Nucleic Acids Res. 2019; 47 D442-D450 [PubMed: 30395289]

Europe PMC Funders Author Manuscripts

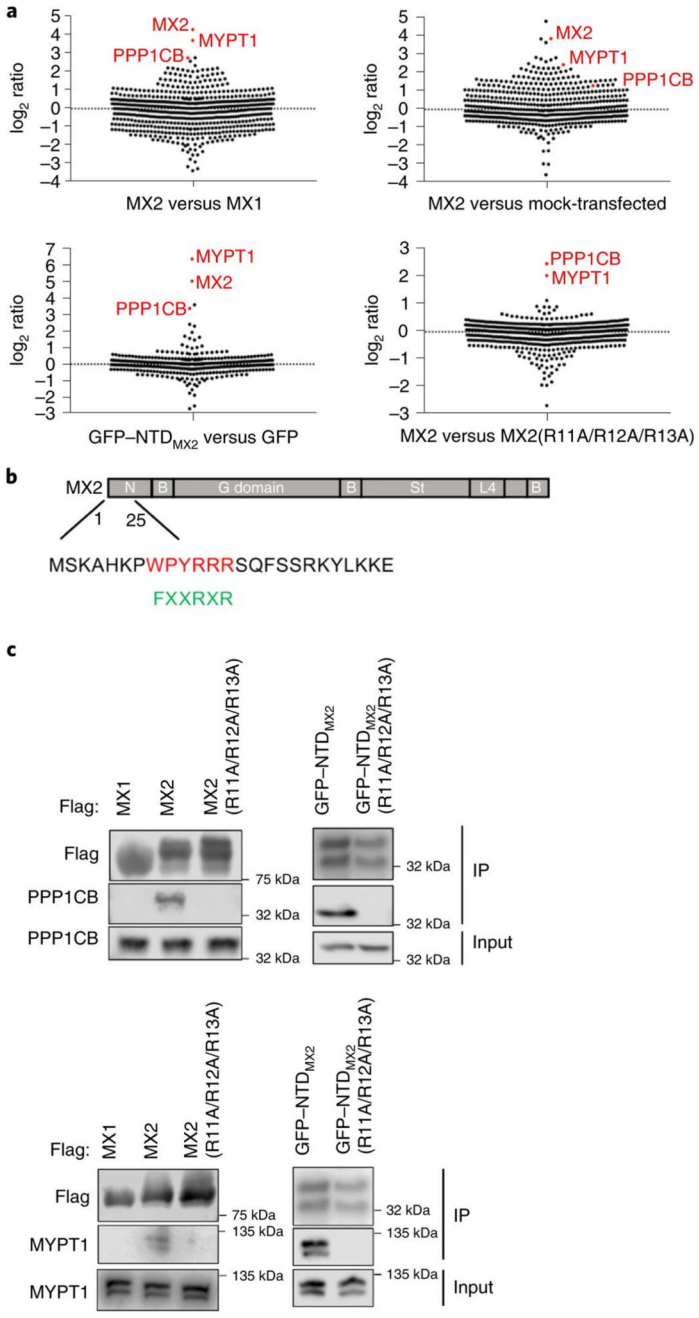


**Fig. 1. The N-terminal domain of MX2 interacts with MYPT1 and PPP1CB**

**a,** Stable isotope labelling by amino acids (SILAC) screen for MX2 binding proteins. Streptavidin-tagged MX2, MX1, MX2 R11-13A, GFP or GFP ($NTD_{MX2}$) were expressed in 293T cells labelled with “light”, “medium” or “heavy” amino acids, immune-affinity purified and analyzed by tandem mass spectrometry. Representative experiments comparing MX2 (medium) versus MX1 (light) (n= 3 biological replicates), MX2 (medium) versus mock (light) transfected cells (n= 1), GFP ($NTD_{MX2}$) (heavy) versus GFP (light) (n= 2

biological replicates) and MX2 (light) versus MX2 R11-13A (medium) (n= 3 biological replicates) are shown. Values on the y-axis are in Log-2 scale.

**b,** MX2 domain organization showing the sequence of the N-terminal 25 amino acids, highlighting the MLCP binding motif (in red) and a consensus PP1 binding sequence (in green).

**c,** Interaction of endogenous PPP1CB (upper panel) or MYPT1 (lower panel) with the MX2 N-terminal domain. Transfected 293T cells expressing Flag-tagged MX1, MX2, MX2 R11-13A, GFP ($NTD_{MX2}$) or GFP ($NTD_{MX2}$) R11-13A were lysed, proteins immunoprecipitated (IP) with an anti-Flag antibody and analyzed by immunoblot using anti-PPP1CB, anti-MYPT1 or anti-Flag antibodies. All experiments were done at least 4 times.



Europe PMC Funders Author Manuscripts

Europe PMC Funders Author Manuscripts

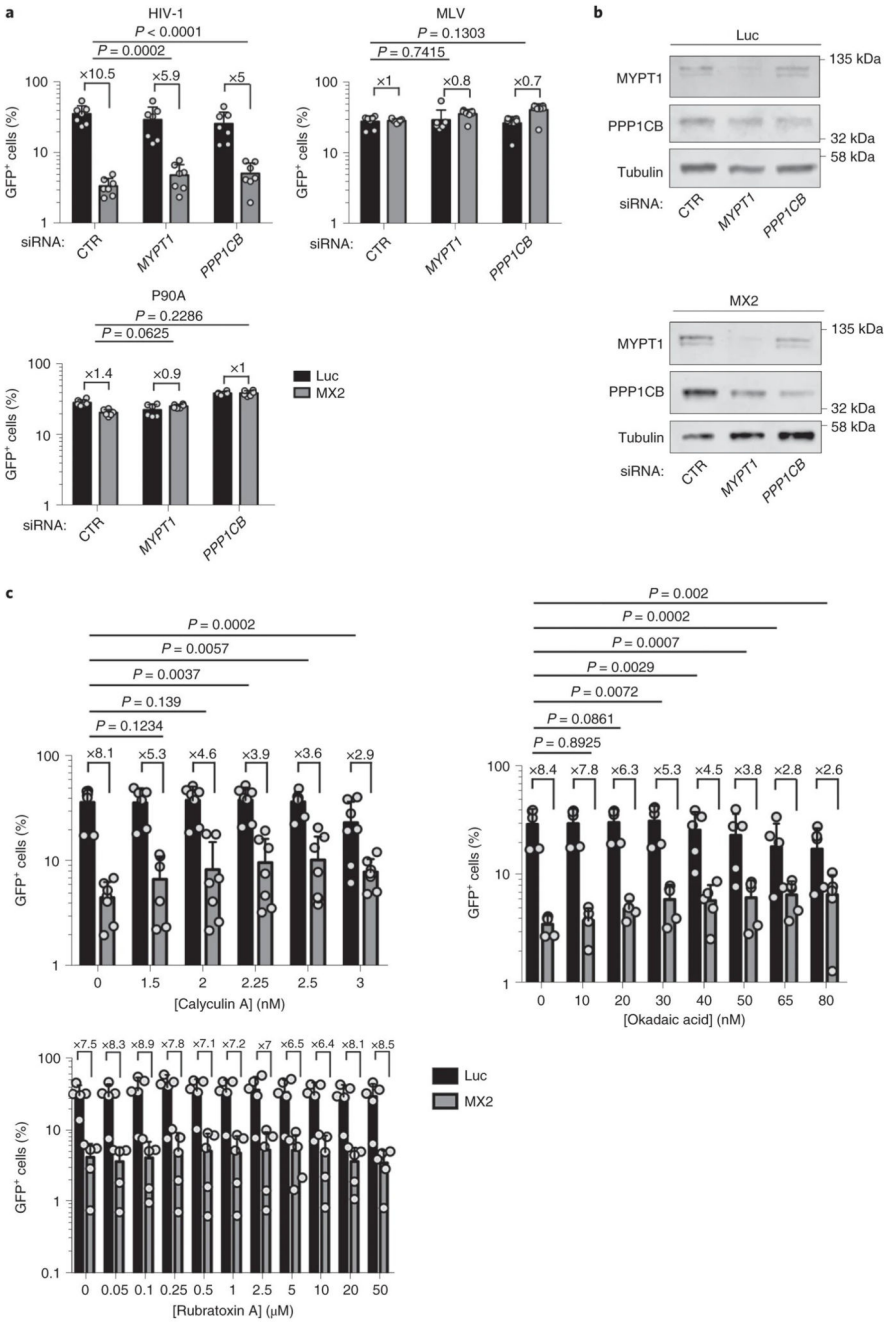


**Fig. 2. MX2 requires functional MLCP for antiviral activity**

**a,** U87-MG CD4$^+$ CXCR4$^+$ cells were transduced with pEasiLV vectors expressing MX2 or the negative control protein Luc and protein expression induced by doxycycline (0.5 μg/ml) for 48 h. MYPT1 or PPP1CB were then depleted by double siRNA transfection. Cells were challenged with wild type or P90A versions of HIV-1/GFP or MLV/GFP and the percentage of infected cells from the pEasiLV transduced population (typically >85%), enumerated at 48 h by flow cytometry (n = 7 biological replicates for HIV-1; n = 6 biological replicates for P90A and MLV, mean ± standard deviation (SD) *p value <0.05; two-tailed unpaired *t*-test).

**b,** Immunoblot analysis of MYPT1 and PPP1CB depletion in U87-MG $CD4^+$ $CXCR4^+$ cells from panel A. Tubulin is included as a loading control.

**c,** U87-MG $CD4^+$ $CXCR4^+$ cells expressing MX2 or Luc were treated with increasing concentrations of calyculin A, okadaic acid or rubratoxin A (or DMSO as a control) 6 h before challenge with HIV-1/GFP. Inhibitors were removed 24 h after addition and the percentage of infected cells enumerated at 48 h by flow cytometry (n = 7 biological replicates for calyculin A; n = 5 biological replicates for okadaic acid and rubratoxin A, mean ± SD, *p value <0.05, (ns) non-significant; two-tailed unpaired *t*-test).



Europe PMC Funders Author Manuscripts

Europe PMC Funders Author Manuscripts

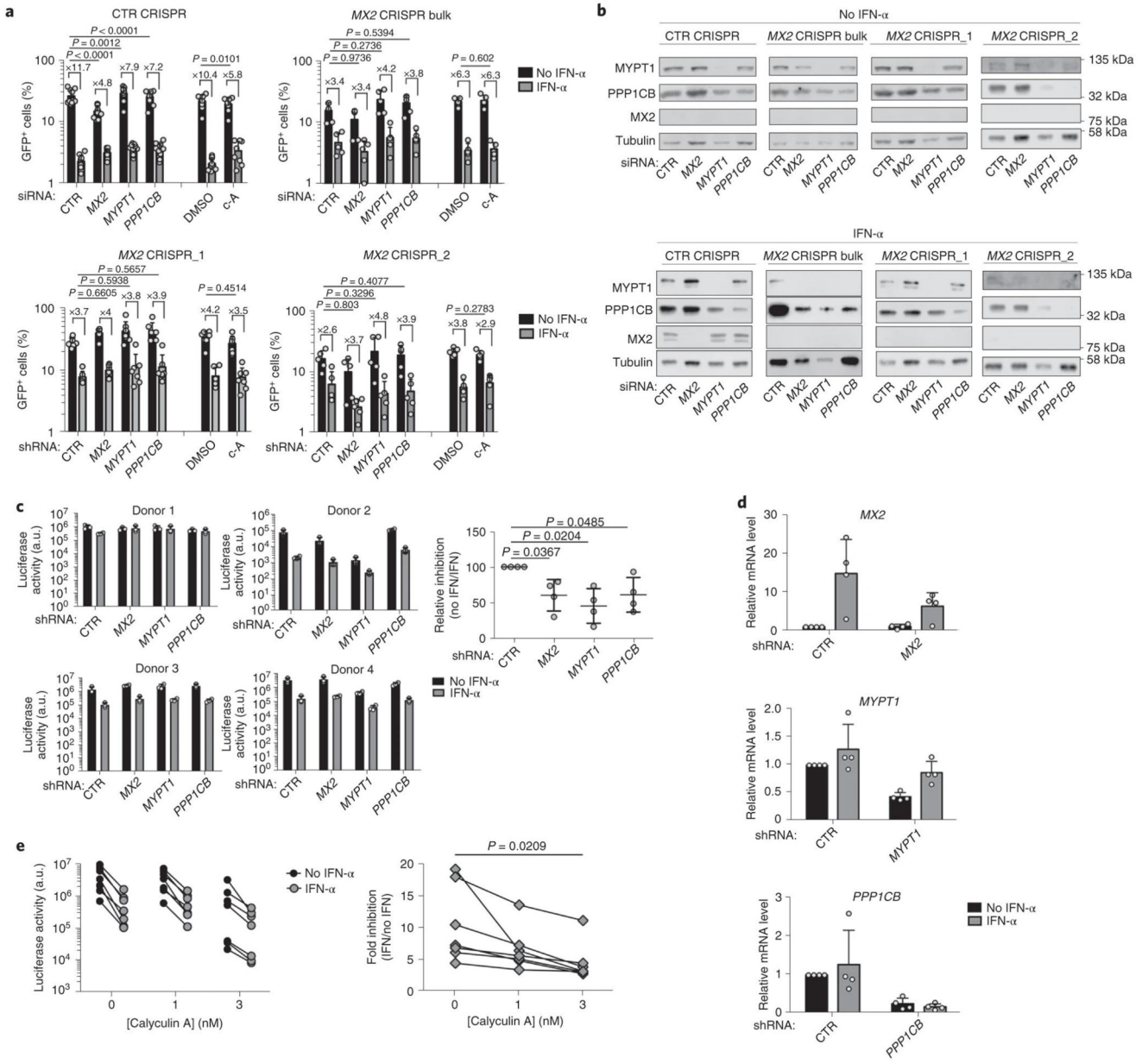


**Fig. 3. Interferon-induced MX2-mediated inhibition of HIV-1 requires MLCP**

**a,** U87-MG CD4$^+$ CXCR4$^+$ cells transduced with a control guide RNA, as well as a bulk population and two clonal cell lines where *MX2* had been disrupted by CRISPR-Cas9 genome editing, were either transfected twice with a control siRNA (CTR), or siRNAs targeting MX2, MYPT1 or PPP1CB, and treated or not with 500 U/ml IFNα for 24 h. Alternatively, cells were treated with 3 nM calyculin A (or DMSO) 6 h before infection and medium exchange 18 h later. Cells were challenged with HIV-1/GFP and infection enumerated at 48 h by flow cytometry (n = 10 biological replicates for CTR CRISPR cells siRNA treatment and n = 8 biological replicates for calyculin A treatment; n = 5 biological replicates for MX2 CRISPR Bulk cells; n = 7 biological replicates for MX2 CRISPR_1

cells; n = 5 biological replicates for MX2 CRISPR_2 cells, mean ± SD, *p value <0.05; two-tailed unpaired *t*-test).

**b,** Immunoblot analysis of MX2, MYPT1, PPP1CB and tubulin (loading control) in CTR CRISPR, MX2 CRISPR Bulk, MX2 CRISPR_1 and MX2 CRISPR_2 cells (from panel A).

**c,** Primary $CD4^+$ T cells were isolated from 4 donors, transduced with shRNAs targeting MX2, MYPT1, PPP1CB or a scrambled sequence shRNA (CTR) and treated or not with 2,000 U/ml IFNα. At 24 h, cells were challenged with NL4.3/Nef-IRES-Renilla and luciferase activity determined 48 h later. Raw infectivity data are shown on the left (mean values from 3 technical replicates), and the fold inhibition of infection (no IFN/IFN) normalized to the CTR shRNA (arbitrary value of 100), on the right (*p-value <0.05; two-tailed paired *t*-test).

**d,** MX2, MYPT1 or PPP1CB depletion in primary $CD4^+$ T cells after shRNA transduction was quantitated by qPCR, normalizing to GAPDH. Data shown represent the donors used in panel C (n = 4, mean ± SD).

**e,** Primary $CD4^+$ T cells treated or not with 2,000 U/ml of IFNα were incubated in the presence of DMSO or two concentrations of calyculin A (1 nm or 3 nM). After 6 h, cells were challenged with NL4.3/Nef-IRES-Renilla and luciferase activity determined after 48 h. Raw infectivity data from all 7 donors are shown on the left and the fold inhibition of infection (no IFN/IFN), on the right (*p-value <0.05; two-tailed paired *t*-test).

Europe PMC Funders Author Manuscripts

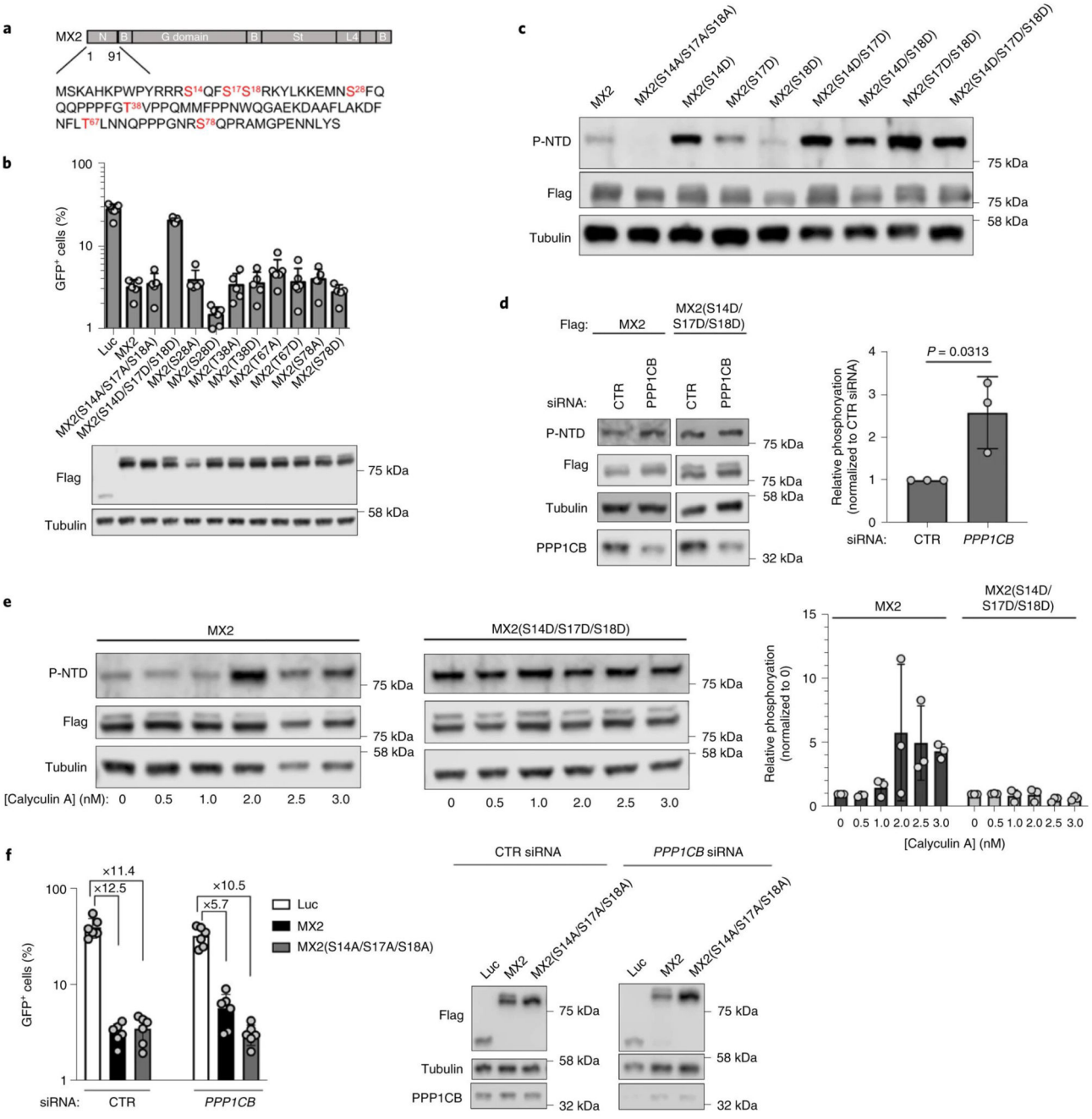


**Fig. 4. MX2 antiviral activity is antagonized by phosphorylation**

**a,** MX2 domain organization showing the sequence of the N-terminal domain, and indicating phosphorylated residues (in red).

**b,** U87-MG CD4$^+$ CXCR4$^+$ cells were transduced with pEasiLV expressing Flag-tagged wild type or mutant MX2, or the Luc control. After induction with 0.5 μg/ml of doxycycline for 48 h, cells were challenged with HIV-1/GFP and infectivity measured 48 h later (n = 5 biological replicates, mean ± SD). The anti-Flag immunoblot shows MX2 expression levels, with tubulin as the loading control.

**c,** Specificity of the anti-phosphorylated S14, 17-18 NTD antibody (anti-P-NTD) defined using cell lysates containing wild type or mutated MX2 proteins. Total protein expression (anti-Flag) is shown with tubulin serving as a loading control (representative from 3 independent experiments).

**d,** MX2 or MX2 S14, 17-18D expressing U87-MG $CD4^+$ $CXCR4^+$ cells were doubly transfected with an siRNA targeting PPP1CB or CTR siRNA. Cells were lysed at 48 h and the levels of MX2 phosphorylated at the S14-S17-S18 motif (anti-P-NTD), total MX2 (anti-Flag) or PPP1CB determined by immunoblot. Tubulin was used as a loading control. Quantification of phosphorylation, relative to the MX2 long isoform and normalized to CTR siRNA, is to the right (n = 3 biological replicates, mean ± SD, *p value <0.05; two-tailed unpaired *t*-test).

**e,** DMSO (0) or increasing concentrations of calyculin A were added to U87-MG $CD4^+$ $CXCR4^+$ cells expressing MX2 or MX2 S14, 17-18D. 6 h after treatment, cells were lysed and MX2 (anti-Flag), MX2 phosphorylated at the S14-S17-S18 motif (anti-P-NTD) or PPP1CB analysed by immunoblot. Tubulin was used as a loading control. Quantification of the level of phosphorylation, relative to the MX2 long isoform and normalized to the DMSO control, is to the right (n = 3 biological replicates, mean ± SD, *p value <0.05; two-tailed unpaired *t*-test).

**f,** U87-MG $CD4^+$ $CXCR4^+$ cells expressing Luc, MX2 or MX2 S14, 17-18A were transfected with a CTR siRNA or a siRNA targeting PPP1CB before HIV-1/GFP challenge, infectivity was measured 48 h later by flow cytometry (n = 6 biological replicates, mean ± SD). The fold inhibition by MX2, relative to Luc, is shown. Fold inhibition for MX2 is significantly lower following PPP1CB siRNA treatment ed cells compared to CTR (x12.5 vs x5.7; P value = 0.0001; two-tailed unpaired *t*-test), but not for MX2 S14, 17-18A (x11.4 vs x10.5; P value = 0.4754; two-tailed unpaired *t*-test). Protein expression was confirmed by immunoblot (right panel).

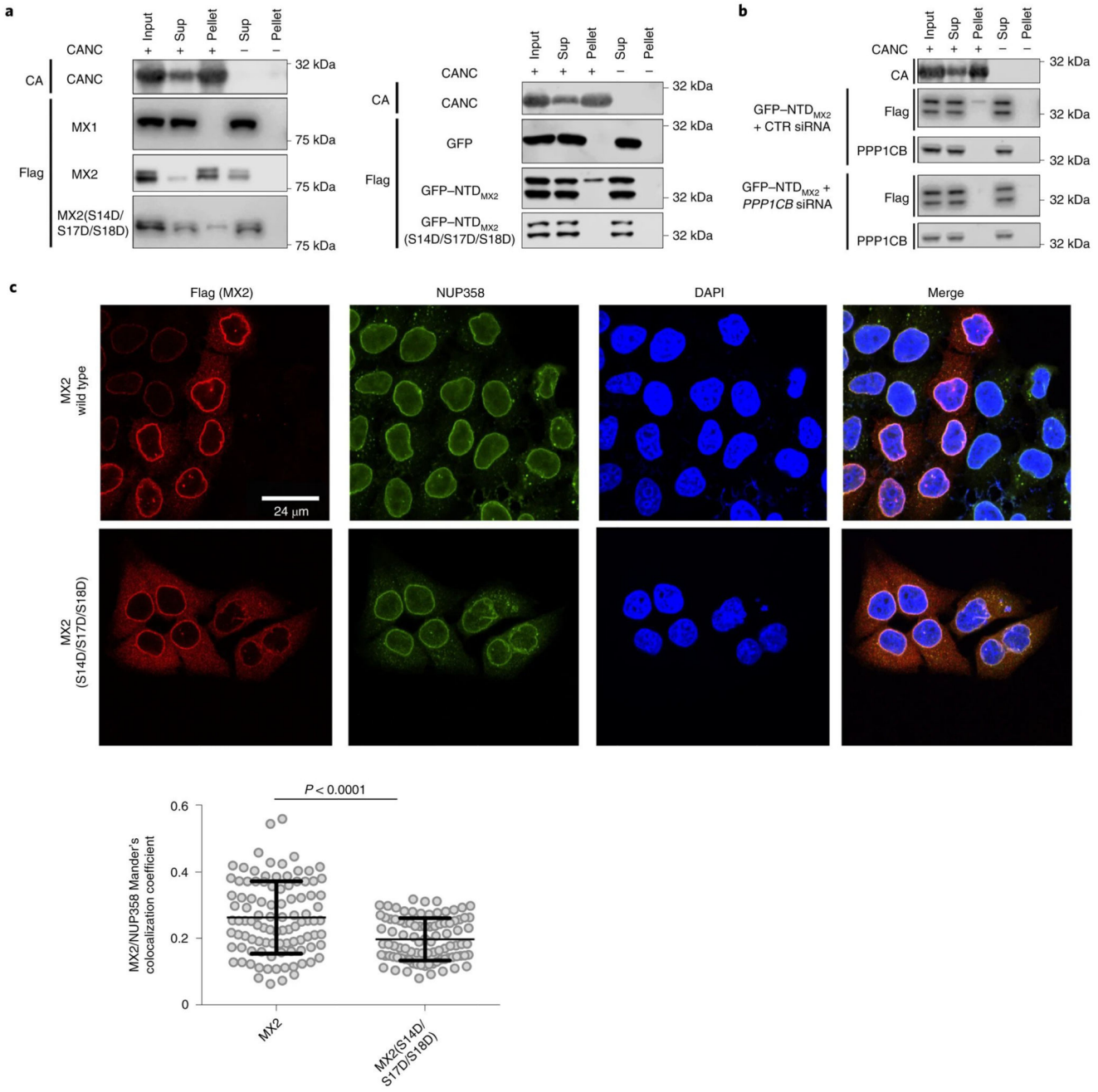


**Fig. 5. Phosphorylation of MX2 reduces HIV-1 capsid binding and nuclear envelope accumulation**

**a,** 293T cells were transfected with pCAGGs vectors expressing Flag-tagged MX1, MX2, mutant MX2 S14, 17-18D, GFP, GFP ($NTD_{MX2}$) or GFP ($NTD_{MX2}$) S14, 17-18D. Cell lysates were incubated in the presence or absence of Capsid-Nucleocapsid (CANC) assemblies and subjected to centrifugation through a sucrose cushion. Supernatant (Sup), Pellet and Input samples were analyzed by immunoblot using an anti-Flag antibody. A representative immunoblot for CANC (anti-CA) is shown. All experiments were done at least 4 times.




Europe PMC Funders Author Manuscripts

**b,** 293T cells expressing GFP ($NTD_{MX2}$) were transfected twice with a CTR siRNA or siRNA targeting PPP1CB, lysed and incubated with CANC assemblies. This mixture was centrifuged and Sup, Pellet and Input samples were analyzed by immunoblot using an anti-Flag antibody. A representative immunoblot for CANC (anti-CA) is shown. PPP1CB depletion was confirmed by immunoblot using an anti-PPP1CB antibody. All experiments were done at least 3 times.

**c,** HeLa cells stably expressing wild type or S14, 17-18D mutant MX2 bearing a C-terminal Flag-tag were seeded onto glass coverslips. Localization of MX2 and endogenous NUP358 were determined by confocal microscopy using anti-Flag and anti-NUP358 antibodies. DAPI was used to stain the nuclei. Below, colocalization of MX2 and NUP358 was quantified using Mander's coefficient for an average of 95 cells per condition, randomly selected (*p-value <0.05; two-tailed unpaired *t*-test)



Europe PMC Funders Author Manuscripts

Europe PMC Funders Author Manuscripts

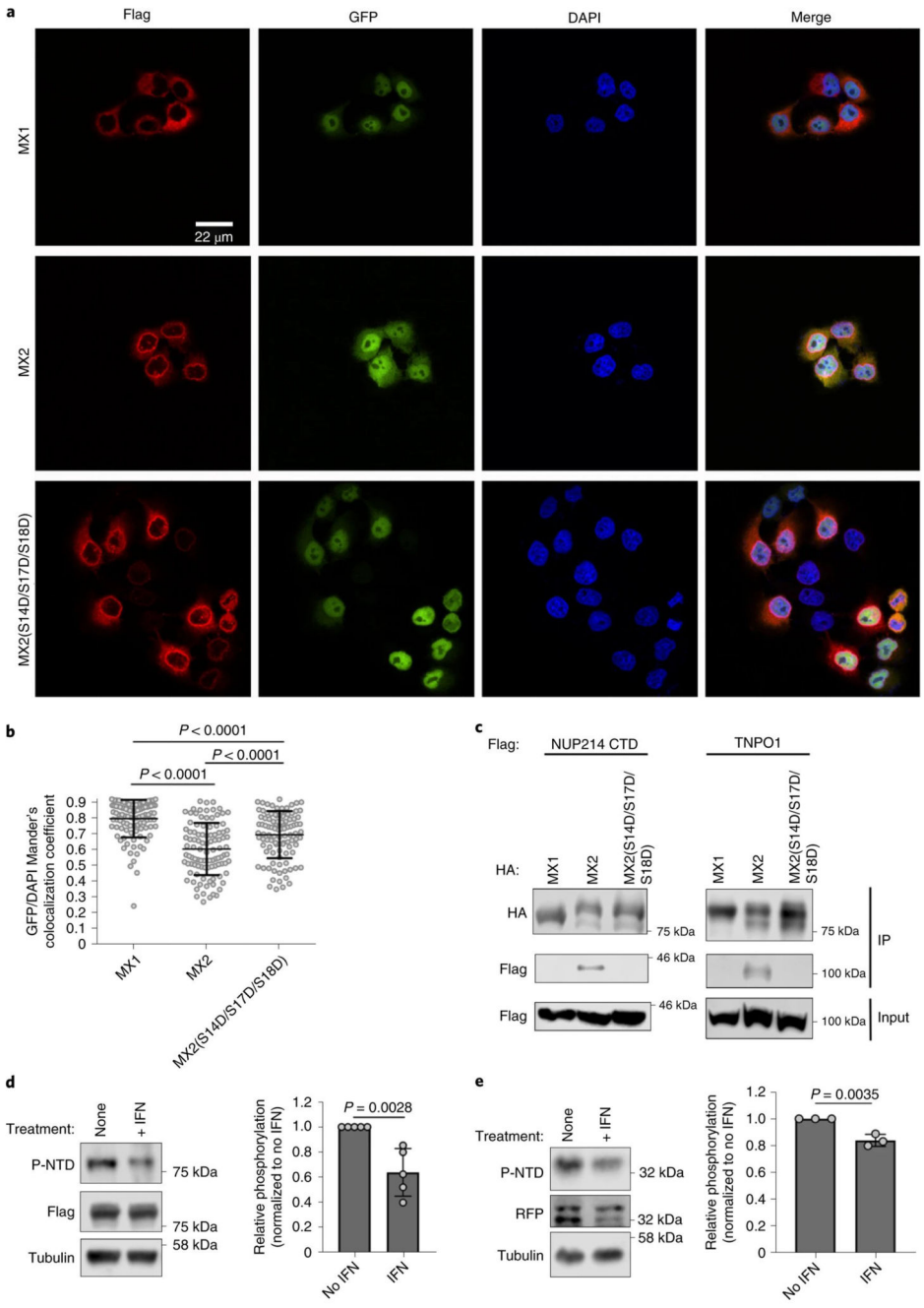


**Fig. 6. MX2-phosphorylation and nuclear import of cellular cargo**

**a,** HeLa cells stably expressing the HNRNP K (KNS)-GFP-LacZ chimera were transduced with puromycinR vectors expressing Flag-tagged MX1, MX2 or MX2 S14, 17-18D and selected for 48 h with puromycin before seeding on glass coverslips. MX proteins were detected using an anti-Flag antibody and the nuclei were stained with DAPI.

**b,** Nuclear localization of KNS-GFP-LacZ was determined for single cells by quantifying colocalization with DAPI using Mander's coefficient for an average of 104 randomly selected cells (*p-value <0.05; two-tailed unpaired *t*-test).

Europe PMC Funders Author Manuscripts

**c,** 293T cells were co-transfected with vectors expressing HA-tagged MX1, MX2 or S14, 17-18D MX2 and Flag-tagged TNPO1 or a C-terminal fragment of NUP214. Cells were lysed and HA-tagged proteins immunoprecipitated and analyzed (together with input samples) by immunoblot using anti-Flag and anti-HA antibodies. All experiments were performed at least 3 times.

**d,** U87-MG $CD4^+$ $CXCR4^+$ cells stably expressing Flag-tagged MX2 were treated or not with 1000 U/ml IFNα for 24 h before lysis and immunoblot analysis with anti-P-NTD or anti-Flag antibodies. Tubulin was used as a loading control. The level of MX2 phosphorylated at the S14-S17-S18 motif, relative to the MX2 long isoform, and normalized to the untreated condition was determined (n =5 biological replicates, mean ± SD, *p-value <0.05; two-tailed unpaired *t*-test).

**e,** RFP bearing the NTD of MX2 (RFP($NTD_{MX2}$)) was expressed in U87-MG $CD4^+$ $CXCR4^+$ cells. Cells were incubated or not with 1000 U/ml IFNα for 24 h, lysed and the level of phosphorylation at the S14-S17-S18 motif, relative to the RFP ($NTD_{MX2}$) long isoform and normalized to the untreated condition, determined as in panel d (n =3 biological replicates, mean ± SD, *p-value <0.05; two-tailed unpaired *t*-test).